Li Jin-hua (Orcid ID: 0000-0003-1622-6170)
Zheng Yue (Orcid ID: 0000-0001-5281-3773)

Diverse phylogeny and morphology of magnetite biomineralized by magnetotactic cocci

Peiyu Liu,[1,2,3,4] Yan Liu,[1,2,3,4] Xiang Zhao,[5] Andrew P. Roberts,[5] Heng Zhang,[1,2] Yue Zheng,[6] Fuxian Wang,[1,2,3,4] Lushan Wang,[7] Nicolas Menguy,[4,8] Yongxin Pan,[1,3,4] Jinhua Li[1,2,4*]

[1]Key Laboratory of Earth and Planetary Physics, Institute of Geology and Geophysics, Innovation Academy for Earth Science, Chinese Academy of Sciences, Beijing 100029, China

[2]Laboratory for Marine Geology, Qingdao National Laboratory for Marine Science and Technology, Qingdao 266061, China

[3]College of Earth and Planetary Sciences, University of Chinese Academy of Sciences, Beijing 100049, China

[4]France-China Joint Laboratory for Evolution and Development of Magnetotactic MultiCellular Organisms, Chinese Academy of Sciences, Beijing 100029, China

[5]Research School of Earth Sciences, Australian National University, Canberra, ACT 2601, Australia

[6]Key Laboratory of Urban Pollutant Conversion, Institute of Urban Environment, Chinese Academy of Sciences, Xiamen 361021, China

[7]State Key Laboratory of Microbial Technology, School of Life Sciences, Shandong University, Qingdao 266237, China

[8]IMPMC, CNRS UMR 7590, Sorbonne Universités, MNHN, UPMC, IRD UMR 206, 75005 Paris, France

*For correspondence. E-mail: lijinhua@mail.iggcas.ac.cn; Tel. (+86) 10 82998323; Fax (+86) 10 62010846

Conflict of interest. The authors declare that they have no conflict of interest.

Running title. Diversity and biomineralization of MTB

2

Abstract. Magnetotactic bacteria (MTB) are diverse prokaryotes that produce magnetic nanocrystals within intracellular membranes (magnetosomes). Here, we present a large-scale analysis of diversity and magnetosome biomineralization in modern magnetotactic cocci, which are the most abundant MTB morphotypes in nature. Nineteen novel magnetotactic cocci species are identified phylogenetically and structurally at the single-cell level. Phylogenetic analysis demonstrates that the cocci cluster into an independent branch from other *Alphaproteobacteria* MTB, i.e., within the *Etaproteobacteria* class in the *Proteobacteria* phylum. Statistical analysis reveals species-specific biomineralization of magnetosomal magnetite morphologies. This further confirms that magnetosome biomineralization is controlled strictly by the MTB cell and differs among species or strains. The post-mortem remains of MTB are often preserved as magnetofossils within sediments or sedimentary rocks, yet paleobiological and geological interpretation of their fossil record remains challenging. Our results indicate that magnetofossil morphology could be a promising proxy for retrieving paleobiological information about ancient MTB.

Keywords. Magnetotactic cocci, Magnetosome, Coordinated FISH-SEM, Morphology, Phylogeny

Summary. Magnetotactic bacteria (MTB) could be the earliest organisms with geomagnetic field-sensing and biomineralizing capability on Earth. Understanding the microbial diversity and biomineralization products of modern MTB is fundamental to

3

developing paleoecological, paleobiological, and paleoenvironmental proxies of their fossil record. Identification of ancient magnetofossils is challenging because the link between microbial phylogeny and biomineralization is not well documented. We present a large-scale analysis that combines microbial phylogenesis and nanoscale mineral characterization to demonstrate a robust relationship between species and morphology of biomineralized magnetite within magnetotactic bacteria. Experimental results provide evidence that magnetosome biomineralization differs among different species or strains. Therefore, magnetofossil morphology is likely to be a promising proxy for retrieving paleobiological information from ancient MTB.

Introduction

Magnetotactic bacteria (MTB) have long been of interest to biologists and geologists because they could represent the earliest geomagnetic field-sensing organisms on Earth (Kopp and Kirschvink, 2008; Uebe and Schüler, 2016; Lin *et al.*, 2017). They are morphologically and phylogenetically diverse prokaryotes that produce intracellularly size-tailored and morphologically-defined nanocrystals of magnetite (Fe_3O_4) or/and greigite (Fe_3S_4) each enveloped by a lipid bilayer membrane called a magnetosome (Bazylinski and Frankel, 2004; Lefèvre and Bazylinski, 2013). Fossil remains of these biominerals (magnetofossils) have been reported widely from Cenozoic sedimentary environments and have been used to retrieve paleomagnetic and tentative paleoenvironmental information (Kirschvink and Chang, 1984; Chang and Kirschvink, 1989; Kopp and Kirschvink, 2008; Roberts *et al.*, 2011; Larrasoaña *et al.*,

4

2014; Savian *et al*., 2014; Savian *et al*., 2016; Sakuramoto *et al.*, 2017; Chang *et al.*, 2018). Studying the biodiversity and biomineralization of MTB is crucial to understand the evolution of iron mineral-based magnetoreception within higher organisms (Lins *et al*., 2006; Lin *et al.*, 2018; Lin *et al.*, 2019; Monteil *et al.*, 2019; Leão *et al.*, 2020). Such studies also provide the principal information needed to develop magnetofossils as novel biogeochemical proxies for simultaneous paleomagnetic, paleoenvironmental, and paleobiological reconstructions (Kopp and Kirschvink, 2008; Jovane *et al*., 2012; Li *et al.*, 2013a; Rodelli *et al*., 2018; Yamazaki *et al.*, 2019; Li *et al*., 2020).

Coccoid-to-ovoid MTB, the so-called magnetotactic cocci, are the most commonly observed morphotypes in natural environments. However, few have been identified and studied, possibly due to the fact that they are fastidious with respect to growth and difficult to distinguish based on their bacterial morphology. So far, only three magnetotactic cocci from marine environments have been cultured axenically: *Magnetococcus marinus* strain MC-1 (Bazylinski *et al.*, 2013), strain MO-1 (Lefèvre *et al.*, 2009), and *Magnetofaba australis* strain IT-1 (Morillo *et al.*, 2014). In addition, despite retrieval of a large number of 16S rRNA gene sequences potentially affiliated with magnetotactic cocci from various environmental samples (Spring *et al.*, 1995; 1998; Lin and Pan, 2009; Kozyaeva *et al.*, 2017; Lin *et al.*, 2018), only a few have been linked unambiguously to a single MTB morphotype (Pan *et al.*, 2008; Lin and Pan, 2009; Kolinko *et al.*, 2013; Abreu *et al*., 2016; Koziaeva *et al.*, 2019). The missing link between bacterial phylogeny and magnetic nanoparticle structure and chain arrangement at the single-cell level (Li *et al.*, 2017; Zhang *et al.*, 2017) hinders

5

understanding of bacterial taxonomy and biomineralization within magnetotactic cocci.

In this study, 19 novel magnetotactic cocci strains from varied freshwater, brackish, and marine environments were identified phylogenetically and structurally using a coupled fluorescence *in situ* hybridization (FISH) and scanning electron microscope (SEM) method developed for single-cell analysis (Li *et al.*, 2017). Together with strain SHHC-1 identified by our group in a previous study (Zhang et al., 2017), the number, size, and morphology of magnetite particles and their chain assembly within these 20 magnetotactic cocci were then determined from detailed transmission electron microscope (TEM) observations. Finally, the relationship between biomineralization and bacterial phylogeny is analyzed statistically. Our large-scale identification of novel magnetotactic cocci strains supports strongly the suggestion that magnetotactic cocci should be reclassified into an independent class in the *Proteobacteria* phylum (Ji *et al.*, 2017; Lin *et al.*, 2018). Our results also test and validate, with the largest assessment available so far, the assumption of species-specific control of magnetosomal magnetite biomineralization within MTB, which provides a foundation for using magnetofossil morphology as a proxy for paleoecological and paleoenvironmental reconstructions.

Results

Bacterial identification and phylogenetic analysis

Fourteen laboratory microcosms dominated by magnetotactic cocci were selected for magnetic enrichment of living MTB cells. According to molecular analyses of 16S rRNA gene sequencing, most cells (79.8%) retrieved from the magnetic enrichments

6

were identified as magnetotactic cocci, along with other MTB and non-MTB types that accounted for 13.3% and 6.9% of cells, respectively (Table S4). Specifically, magnetic enrichments from two microcosms likely contain only one magnetotactic coccus type based on 16S rRNA gene sequence analyses. They were collected from Shihe Estuary (Microcosm-12) and Laolongtou Bay (Microscosm-14). Both are dominant by coastal sandy sediments. In contrast, the other twelve microcosms are dominant by argillaceous sediments due to that they were collected from one tidal flat environment (Microscosm-13) and lake or river environments (Microcosms 1-11) (Table S1). They contain diverse MTB (magnetotactic cocci and other MTB types) and non-MTB species (Table S4). This result indicates a general coexistence of phylogenetically diverse MTB in nature. It also indicates that the widely used method of magnetic separation of MTB from sediments does not avoid contamination by non-MTB cells. Therefore, considering the generally complex composition of MTB in nature or laboratory microcosms, it is necessary to link a targeted 16S rRNA gene to a specific MTB morphotype at single-cell scale. With the help of the recently-developed coupled FISH-SEM approach (Li *et al.*, 2017), we then identified 19 types of magnetotactic cocci from these 14 enriched samples.

As shown in Figure 1, targeted MTB were hybridized with both the EUB338 universal bacterial probe (green) and the corresponding species-specific MTB probe (red), while others (including other types of MTB, non-MTB, and inner control cells of *E. coli* or *Magneospirillum magneticum* AMB-1) were only hybridized with the EUB338 probe. Subsequent coordinated SEM observations on the fluorescence-labeled

bacteria further reveal the detailed morphological and structural features of both cells and their intracellular magnetosomes. With this strategy, we identified 16 magnetotactic cocci from freshwater environments (strains YQC-1, YQC-2, YQC-3, THC-1, BHC-1, MYC-3, MYC-4, MYC-5, MYC-7, DMHC-1, DMHC-2, DMHC-6, DMHC-8, WYHC-1, WYHC-2, and WYHC-3), two from marine environments (strains XJHC-1 and LLTC-1), and one from a brackish environment (strain SHHC-2). Based on FISH-SEM analyses, the cells identified here can be classified into four groups according to their magnetosome chain configuration: single chain, double-separated chains, double parallel chains, and particle aggregates (Figure 1). Careful observations on more target cells demonstrated that for all the cells hybridized by one species-specific oligonucleotide probe contain magnetosomes with identical chain arrangement (Supplementary material S1).

Phylogenetic analysis from 16S rRNA gene sequences indicate that all 19 magnetotactic cocci have a common sequence identity lower than 97%, so they can be assembled as different species in the phylogenetic tree (Fig. 2A). Further sequence alignment reveals that eight of the magnetotactic cocci (strains MYC-3, MYC-7, DMHC-1, DMHC-8, YQC-1, YQC-3, THC-1, and LLTC-1) have high similarity (97-99% for different strains) to previously known 16S rRNA sequences (Table 1) (Spring *et al.*, 1998; Flies *et al.*, 2005b; Lin *et al.*, 2009; Lin and Pan, 2010; Wang *et al.*, 2013; Chen *et al.*, 2015). The other 11 magnetotactic cocci may represent novel species due to sequence identities lower than 97% with respect to known sequences. TEM observation was carried out following the coupled FISH-SEM analyses. Phylogenic tree

8

and representative TEM images of all 19 magnetotactic cocci are shown in Figure 2.

Chemical and morphological characterization

TEM observations reveal that most of the magnetotactic cocci have spherical morphologies except for a few ovoid cocci (e.g., WYHC-2 (Fig. 2H) and DMHC-1 (Fig. 2J)), with average sizes ranging from ~1.0 to ~2.5 µm. Most magnetotactic cocci contain more than 10 magnetite particles per cell. In contrast, strains DMHC-6 (Fig. 2S) and WYHC-2 (Fig. 2H) produce relatively more magnetosomal particles, i.e., averages of 70±13 and 103±16 particles per cell, respectively (Table 1). Energy dispersive X-ray (EDX) spectroscopy coupled with scanning TEM (STEM) observations demonstrate that these particles are rich in iron and oxygen, which indicates that the studied magnetotactic cocci biomineralize magnetosomal magnetite crystals (Fig. S1).

The chain configuration and crystal morphology of magnetosomes within each MTB species were investigated in detail by TEM observations (Fig. 2, Table 1). Magnetite particles are arranged into a single chain in strains YQC-1, BHC-1, YQC-2, DMHC-1, WYHC-1, and WYHC-3 (Fig. 2B-D, J, K, T), whereas double separated chains occur in strains MYC-4, XJHC-1, LLTC-1, MYC-5, and YQC-3 (Fig. 2E-G, M, O), and two double chains occur in strains DMHC-8 and DMHC-2 (Fig. 2N, P). Magnetite particles within the other six strains are not arranged into linear single or multiple chains and consist of dispersed aggregates (strains WYHC-2, THC-1, MYC-3, and MYC-7; Fig. 2H, L, Q, R), dispersed aggregates and partial chains (strain DMHC-6; Fig. 2S), and particle clusters and partial chains (strain SHHC-2; Fig. 2U).

9

Despite having nearly identical chain configuration in all cells for each MTB species, there is no obvious correlation between the phylogenetic relatedness and the chain arrangement. This indicates that the chain configuration of magnetosomes is important but not unique feature for distinguishing different MTB.

Most of the studied magnetotactic cocci strains produce elongated prismatic projections with axial ratio (i.e., width/length) values lower than 0.8, except for strains MYC-5 and WYHC-3, which produce octahedral and cubo-octahedral magnetite morphologies, respectively (Figs. S2-S5). Strain DMHC-2 appears to form elongated cubo-octahedral magnetite crystals (Figure S4). Our previous study has shown that strain SHHC-1 forms elongated octahedral magnetite crystals (Zhang *et al.*, 2017). Nevertheless, crystal sizes and their axial ratios are different (Table 1). Statistically, each strain appears to produce magnetite particles with their own crystal size and shape distributions (Fig. 3). A two-dimensional Kolmogorov–Smirnov test confirms that the magnetite morphologies are statistically different among the magnetotactic cocci (Supplementary material S2).

Despite their structural and morphological diversity, magnetite particles produced by these magnetotactic cocci share common features, as observed in other cultured and uncultured MTB that produce prismatic, octahedral, or cubo-octahedral magnetite particles (Devouard *et al.*, 1998; Li *et al.*, 2013b; Pósfai *et al.*, 2013). For instance, structural and morphological features of magnetite within the same magnetotactic coccus strain are uniform, i.e., identical chain configuration and narrow particle number distribution (Fig. 3, Figs. S2-S5). Crystal length and width distributions are all skewed

10

negatively with skewness values ranging from -0.57 to -1.47 for length and from -0.44 to -1.34 for width. In addition, the magnetite crystals have relatively narrow size distributions with average lengths ranging from ~60 to ~114 nm and an average width from ~36 to 86 nm, which fall within the magnetically ideal size range for stable single domain (SD) particles (Fig. S6) (Muxworthy and Williams, 2009). These observations confirm that chain configurations and crystal morphologies are diverse in MTB, but that they are homogeneous for a given MTB species or strain (Pósfai *et al.*, 2013).

Notably, magnetotactic cocci appear to organize their magnetosomal magnetite particles in a relatively more complicated way compared to other MTB (e.g., Kobayashi *et al*., 2006). The spatial arrangement of magnetite magnetosomes within magnetotactic cocci, particularly with non-chain structure and corresponding molecular mechanisms, deserve further study by electron tomography and comparative genomics (e.g., Zhang *et al*., 2017; Lin *et al*., 2018). In addition, consistent with previous studies (Mann *et al*., 1984; Meldrum *et al*., 1993a, Meldrum *et al*., 1993b; Li *et al*., 2013b; Li *et al*., 2017; Zhang *et al*., 2017), small (immature) magnetite particles are often observed at the ends of magnetosome chains within most magnetotactic cocci. However, tiny magnetite particles can also be distributed outside magnetosome chains within strain LLTC-1, resulting in a particularly long tail with smaller length and width distributions (Fig. 3B). This may suggest that magnetic particles within strain LLTC-1 grow gradually.

Discussion and conclusions

Diversity and taxonomic position of magnetotactic cocci

11

The taxonomic position of magnetotactic cocci has long been debated, despite their widespread detection in natural environments since the mid-1970s (Blakemore, 1975; Lefèvre and Bazylinski, 2013). Early cultivation-independent studies based on phylogenetic analysis of 16S rRNA genes proposed that magnetotactic cocci are affiliated within the *Alphaproteobacteria*, but that they form a separate lineage (Spring *et al.*, 1992; Delong *et al.*, 1993; Spring *et al.*, 1995; Spring *et al.*, 1998; Flies *et al.*, 2005a), or represent the earliest-diverging *Alphaproteobacteria* branch (Esser *et al.*, 2007; Bazylinski *et al.*, 2013). Conversely, one early study suggested that *Magnetococcus marinus* MC-1 should be assigned to a novel *Proteobacteria* subdivision because it appears to be related more closely to the class *Zetaproteobacteria* based on a phylogenetic tree of 16S rRNA genes (Singer *et al.*, 2011). From comparative genomic and metagenomic studies of both cultured and uncultured MTB, two recent studies further proposed that magnetotactic cocci might represent a novel monophyletic class of *Proteobacteria* (i.e., "*Candidatus* Etaproteobacteria") (Ji *et al.*, 2017; Lin *et al.*, 2018). However, most investigators insist that magnetotactic cocci should be clustered into a new order *Magnetococcales*, which represents the basal-most lineage within the *Alphaproteobacteria*, because the overall topologies of these phylogenetic trees are based on a limited number of data that preclude definitive determination of the taxonomic position of magnetotactic cocci (Bazylinski *et al.*, 2013; Lefèvre and Bazylinski, 2013).

The three axenically cultured magnetotactic cocci strains all produce a few to a dozen magnetite particles that are arranged into a single intracellular chain (Lefèvre *et*

12

al., 2009; Bazylinski *et al.*, 2013; Morillo *et al.*, 2014). Magnetotactic cocci are generally small and spherical or ovoid. They are not easy to identify unambiguously using traditional molecular ecology techniques and fluorescence microscopy (Li *et al.*, 2017). Our FISH-SEM approach couples fluorescence and electron microscope observations on the same bacteria targeted with fluorescently labelled oligonucleotide probes, and has proven to be practicable for single-cell phylogenetic and structural identification of uncultivated MTB from complex and diverse microbial communities in environmental samples (Li *et al.*, 2017; Zhang *et al.*, 2017; Li *et al.*, 2019; Qian *et al.*, 2019; Qian *et al.*, 2020). This study is the first to identify and analyze large numbers of magnetotactic cocci from varied aquatic environments using the coupled FISH-SEM method and TEM characterization. Our results provide substantial evidence to better understand bacterial diversity and the taxonomic position of magnetotactic cocci, as well as magnetite biomineralization within them. As shown in Figure 4, phylogenetic analyses based on 16S rRNA gene sequences indicate that all 19 identified strains cluster into an independent phylogenetic branch along with several previously reported magnetotactic cocci, which are related distantly to the *Alphaproteobacteria*, *Gammaproteobacteria, Betaproteobacteria*, *Deltaproteobacteria*, and *Epsilonproteobacteria* in the *Proteobacteria* phylum.

Different from morphologically diverse MTB within other classes or phyla, all bacteria affiliated with the *Etaproteobacteria* identified so far have spherical or ovoid cell morphologies. Also different from the co-classification of non-MTB and MTB within other classes or phyla, the bacteria discovered so far from the *Etaproteobacteria*

13

class are all MTB (Fig. 4). This suggests that the *Etaproteobacteria* might consist only of magnetotactic cocci. One interpretation of this observation is that the magnetosome gene cluster (MGC, i.e., the genes responsible for magnetosomal biomineralization) within magnetotactic cocci is more stable than in other MTB due to a lack of transposable elements around or within the MGC (Schübbe *et al.*, 2009; Morillo *et al.*, 2014; Ji *et al.*, 2017; Lin *et al.*, 2018). Alternatively, it is possible that non-MTB species affiliated with the *Etaproteobacteria* class exist in natural environments, which needs more extensive survey. In addition, comparative genomic analysis reveals that the genomes of magnetotactic cocci strains MC-1 and MO-1 have a mosaic origin affiliated with *Alphaproteobacteria*, *Betaproteobacteria*, *Gammaproteobacteria*, *Deltaproteobacteria*, or *Epsilonproteobacteria* (Ji *et al.*, 2017). This suggests that the *Etaproteobacteria* class may represent a transition between the *Deltaproteobacteria* and the *Alphaproteobacteria*, *Betaproteobacteria*, *Gammaproteobacteria*, or even an ancestor of the *Proteobacteria* phylum. Further genomic analyses on the uncultured magnetotactic cocci identified here will provide more clues to better understand the origin and evolution of MTB and of magnetoreception within MTB.

Relationship between magnetite biomineralization and bacterial phylogeny

Our study demonstrates that magnetosomal magnetite biomineralization (e.g., chain configuration, particle number, crystal size, and morphology) within magnetotactic cocci is diverse (Fig. 2, Table 1). To understand the relationship between magnetite biomineralization and MTB species, non-metric multidimensional scaling

14

(nMDS) analysis was carried out on four main aspects, including chain configuration, particle number, crystal width, and axial ratio (Fig. S7). As shown in Figure 5, nMDS analysis indicates that data for all cells from the same MTB species tend to gather together in the nMDS plot, and that data for different MTB species are relatively dispersed from each other. Permutational multivariate analysis (PERMANOVA) based on the nMDS results further reveals that the difference in magnetite biomineralization between two random MTB species is significant ($P<0.001$, Supplementary material S3).

The nature of chain configurations contributes dominantly to the nMDS results for all MTB species with proportion of variance up to ~84%, so that MTB species with the same chain configuration cluster into a separate region from others (Fig. 5). For MTB species with no chains, the number of magnetite particles per cell contributes dominantly with proportion of variance up to ~84%. For the three other chain configurations, crystal width or axial ratio provide a primary contribution with proportion of variance up to ~61% (Supplementary material S3). It has been demonstrated that biomineralization within MTB is strictly controlled genetically, and that features such as chain arrangement, particle number, crystal size, and morphology are related directly or indirectly to certain genes within its MGC (Murat *et al.*, 2010; Komeili, 2012; Uebe and Schüler, 2016). The *mamK*, *mamJ*, and *mamY* genes are responsible for chain construction within magnetotactic spirilla (strains AMB-1 and MSR-1) (Scheffel *et al.*, 2006; Katzmann *et al.*, 2010; Toro-Nahuelpan *et al.*, 2019). The *mamC*, *mamD*, *mamG*, *mamF*, and *mms6* genes are related to crystal size and morphology (Scheffel *et al.*, 2008; Staniland and Rawlings, 2016), while *mamA*, *mamP*,

15

mam*T*, and *mamS* are associated with the number of particles (Komeili *et al.*, 2004; Murat *et al.*, 2010; Siponen *et al.*, 2013; Uebe and Schüler, 2016). In contrast to *Magnetospirilla*, only several core genes (mamABFKMOPI) are observed on the MGCs of three cultured magnetotactic cocci (strains MC-1, MO-1, and IT-1) and one uncultured strain (*Ca.* Magnetaquicoccus inordinatus UR-1) (Schübbe *et al.*, 2009; Morillo *et al.*, 2014; Ji *et al.*, 2017; Koziaeva *et al.*, 2019). Therefore, the copy number variation and divergence of these core genes or/and other unknown genes in the MGCs of different MTB species may result in diverse biomineralization within magnetotactic cocci, which also needs further genomic study.

Direct analysis of magnetofossil morphology in the ancient sedimentary record is being used increasingly to reconstruct paleoenvironments (Yamazaki and Kawahata, 1998; Egli, 2004; Usui *et al.*, 2017; Chang *et al.*, 2018; Yamazaki *et al.*, 2019; He and Pan, 2020). Yamazaki and Kawahata (1998) found that magnetofossils in Pacific deep-sea sediments are more isotropic in more oxidizing paleo-conditions and are more anisotropic in more reducing environments. Chang *et al.* (2018) reconstructed a deep-sea ecological pattern of coupled MTB increases with an oxygenation decline during the Paleocene–Eocene Thermal Maximum (PETM) through quantifying magnetofossil abundance and morphology from the PETM onset to its peak at Walvis Ridge, South Atlantic Ocean. Studies of modern MTB indicate that the distribution, presence, and abundance of MTB are affected by environmental parameters such as salinity, oxygen, temperature, or sulfur compounds (e.g., Lin *et al.*, 2014). The crystal morphology of biogenic magnetite is associated with MTB phylogenetic group (Pósfai *et al.*, 2013).

16

For example, MTB affiliated with *Etaproteobacteria*, *Alphaproteobacteria*, and *Gammaproteobacteria* produce magnetosomal magnetite with octahedral, cubo-octahedral, or elongated prismatic shapes (Mann *et al.*, 1984; Meldrum *et al.*, 1993a, Meldrum *et al.*,1993b; Li *et al.*, 2013b; Li *et al.*, 2017; Zhang *et al.*, 2017), while MTB in the class *Deltaproteobacteria*, *Nitrospirae*, and *Omnitrophica* produce highly elongated anisotropic magnetite crystals (Pósfai *et al.*, 2006; Lefèvre *et al.*, 2011; Kolinko *et al.*, 2012; Li *et al.*, 2015; Li *et al*., 2020). Our results further demonstrate that a combination of physical features (i.e., chain configuration, particle number, crystal morphology, and size) can distinguish MTB groups even at species or strain level. This indicates that comprehensive analysis of chain assembly, particle number, crystal morphology, and size should provide a robust basis for MTB classification and magnetofossil identification. To do this, systematic study of the relationship between bacterial phylogeny, magnetite biomineralization, and environmental factors (e.g., salinity, oxygen, temperature, and pH) in modern MTB is required urgently to develop the use of magnetofossils as a biogeochemical proxy, i.e., to retrieve information about the environments in which ancient MTB lived. In concert, larger scale studies of MTB in various environments are needed to develop a much more extensive database of phylogenetic information coupled with nanoscale characterization of physical aspects of the magnetite biomineralized by MTB.

In summary, we present a large-scale bacterial characterization of magnetosomal magnetite from wild-type magnetotactic cocci. In total, 19 novel strains were identified phylogenetically and structurally for the first time using a coupled FISH-SEM approach

at the single-cell level. Phylogenetic analysis demonstrates that these strains cluster into an independent branch from other *Alphaproteobacteria* MTB, which supports strongly the idea that the order *Magnetococcales* should become a new class, i.e., the *Etaproteobacteria* class in the *Proteobacteria* phylum (Ji *et al.*, 2017; Lin *et al.*, 2018). Systematic TEM observations demonstrate diverse magnetite biomineralization among magnetotactic cocci strains in terms of particle number, crystal size, axial ratio, and chain configuration, whereas these variables are generally homogeneous for a given species. Statistical analysis between bacterial phylogeny and magnetite biomineralization further reveals species-specific biomineralization, which indicates that magnetite production is controlled strictly by the MTB cell with different morphologies produced by different species or strains. Further extensive studies of the diversity and ecology of modern MTB, coupled with detailed characterizations of the size/shape/arrangement of their biomineralized magnetite, are needed to build on the foundation provided here to develop biogeochemical paleoenvironmental proxies from the magnetofossil record.

Materials and methods

Sediment sampling, MTB collection, and sample preparation

Surface sediments were collected from nine locations from freshwater, brackish, and marine environments in China (Table S1). The collected sediments were transferred into 500-ml plastic bottles with a 2:1 sediment to water ratio. The bottles were shipped to the laboratory and were stored at ~20°C in dim light to set up the laboratory

18

microcosms. MTB in the microcosms were checked routinely with the hanging-drop technique (Schüler, 2002) using an Olympus BX51 microscope equipped with phase-contrast, fluorescence, and a DP70 digital camera system (Olympus Corp., Tokyo, Japan). Sufficient living MTB cells of interest were extracted magnetically from the sediments, washed three times with Milli-Q water, and were then divided into three parts for TEM, molecular, and FISH-SEM experiments, respectively, following the protocol of Li *et al.* (2017).

Molecular experiments

PCR amplification of 16S rRNA genes of MTB cells was performed using the universal bacterial primers 27F (5-′AGAGTTTGATCCTGGCTCAG-3′) and 1492R (5′-GGTTACCTTGTTACGACTT-3′) (Lane, 1991), following the protocol of Li *et al.* (2017). PCR products were purified using an EZNAR Gel Extraction Kit (Omega Bio-tek, Inc., USA). They are ligated with the pMD19-T vector (TaKaRa, Japan), then cloned in *Escherichia coli* (strain DH5α) competent cells (Tiangen, Beijing, China) according to the manufacturer's instructions. For each microcosm, 10-80 clones were picked randomly and were sequenced using the vector primers M13-47 (5′-CGCCAGGGTTTTCCCAGTCACGAC-3′) and RV-M (5′-GAGCGGATAACAATTTCACACAGG-3′) at the Huada Genome Center (Beijing, China). After discarding sequences of insufficient length (<1,300 bp), remaining sequences were aligned with close relatives using the ClustalW algorithm for manual correction. A phylogenetic tree was constructed using the maximum likelihood (ML) method (Tamura and Nei, 1993) in the MEGA software package (version 7.0) (Kumar

19

et al., 2016). Bootstrap values were calculated with 1,000 replicates.

Coupled FISH-SEM experiments and MTB identification

Nineteen species-specific oligonucleotide probes were designed to target specifically the corresponding 16S rRNA genes of magnetotactic cocci identified in this study (Table S2). Their probe specificity is given in Table S3. The universal bacteria probe EUB338 (5′-GCTGCCTCCCGTAGGAGT-3′) was used as a positive control probe of bacteria for FISH (Amann *et al.*, 1990; Li *et al.*, 2017). Probe EUB338 was synthesized and fluorescently labeled with fluorescein phosphoramidite FAM at the 5′ end, while all MTB species-specific probes were synthesized and labeled fluorescently with hydrophilic sulfoindocyanine dye Cy3 at the 5′ end. In some cases, *E. coli* or/and *Magnetospirillum magneticum* AMB-1 cells were added in appropriate amounts to the targeted magnetotactic cocci as inner control cells of non-magnetotactic *Gammaproteobacteria* or/and magnetotactic *Alphaproteobacteria*, respectively (Li *et al.*, 2017). Coupled FISH-SEM analysis was performed using the protocol described by Li *et al.* (2017). Fluorescence microscopy experiments were carried out using an Olympus BX51 microscope. After fluorescence microscope observations, the same sample was carbon-coated using a Leica ACE200 Low Vacuum Sputter Coater (Leica Microsystems, Wetzlar, Germany), and was observed using a Zeiss Ultra-55 field-emission gun SEM (Carl Zeiss, Germany) operating at 5 kV.

TEM Analysis

Conventional TEM observations were performed on a JEM2100 microscope (JEOL Ltd., Tokyo, Japan) operating at 200 kV at the Institute of Geology and

20

Geophysics, Chinese Academy of Sciences (Beijing, China). Cell diameter, particle number, and crystal length (along the long axis) and width (perpendicular to the long axis) of the magnetite particles were measured from the TEM images of individual MTB cells. The axial ratio of particles is the width/length ratio. For each MTB strain, at least 30 individual cells were selected randomly for statistical analysis of cell diameter and particle number, with at least 300 individual particles selected randomly for statistical analysis of crystal length and width. Chemical microanalysis was carried out with a JEM-2100F microscope (JEOL Ltd., Tokyo, Japan) operating at 200 kV at the Institut de minéralogie, de physique des matériaux et de cosmochimie (Paris, France). This microscope is equipped with a field emission gun, a JEOL detector with an ultrathin window, and a scanning TEM device. EDX elemental mapping was carried out in high-angle annular dark-field STEM mode.

Data processing and statistical analysis

Probability distribution analysis and 2D Kolmogorov-Smirnov tests were used to analyze crystal lengths, widths, and axial ratios to estimate differences in particle morphology among MTB species. To study quantitively the relationship between bacterial phylogeny and magnetosome biomineralization, nMDS analysis was performed using four physical features (particle number, chain configuration, crystal width, and axial ratio) using vegan, a package of community analysis functions for the statistical software R. NMDS is a rank-based method in which the original distance is substituted with ranks. The ranks of particle number, crystal width, and axial ratio for one certain MTB cell are obtained by normalized to the corresponding maximum values

21

within all the test cells. For the chain configuration, the rank for two double chains, two chains, single chain, and non-chain were designed to 1.0, 0.5, 0.25, and 0, respectively. Permutational analysis of variance (PERMANOVA) (Anderson, 2001) was used to test for differences in magnetite biomineralization among MTB species. Envfit was further used to fit biomineralization vector features onto the nMDS ordination to determine average factor levels.

Data availability. The 16S rRNA gene sequences obtained here have been deposited in GenBank. Magnetotactic cocci strains MYC-3, MYC-4, MYC-5, MYC-7, DMHC-1, DMHC-2, DMHC-6, DMHC-8, WYHC-1, WYHC-2, WYHC-3, YQC-1, YQC-2, YQC-3, BHC-1, LLTC-1, SHHC-2, THC-1, and XJHC-1 are under accession numbers MN372077, MN372080, MN396678, MN396679, MN396579, MN396560, MN396584, MN396585, MN396452, MN396580, MN396581, MN396453, MN396538, MN396541, MN396586, MN396600, MN396451, MN396570, and MN396582, respectively.

Author contributions. JHL designed the research. PYL, YL, HZ, and FXW prepared samples and carried out microbiological experiments. JHL, PYL, and NM carried out TEM experiments. JHL, PYL, HZ, and FXW performed FISH-SEM experiments. JHL, PYL, XZ, YZ, and YL carried out data and statistical analysis. All authors participated in discussion of results. JHL and PYL prepared the manuscript.

References

Abreu, F., Carolina, A., Araujo, V., Leao, P., Silva, K. T., De Carvalho, F. M., Cunha, O. D. L., Almeida, L. G., *et al.* (2016) Culture-independent characterization of novel psychrophilic magnetotactic cocci from Antarctic marine sediments. Environ Microbiol **18**: 4426-4441.

Amann, R. I., Krumholz, L. and Stahl, D. A. (1990) Fluorescent-oligonucleotide probing of whole cells for determinative, phylogenetic, and environmental studies in microbiology. J Bacteriol **172**: 762-770.

Anderson, M. J. (2001) A new method for non-parametric multivariate analysis of variance. Austral Ecol **26**: 32-46.

Bazylinski, D. A. and Frankel, R. B. (2004) Magnetosome formation in prokaryotes. Nat Rev Microbiol **2**: 217-230.

Bazylinski, D. A., Williams, T. J., Lefèvre, C. T., Berg, R. J., Zhang, C. L. L., Bowser, S. S., Dean, A. J. and Beveridge, T. J. (2013) *Magnetococcus marinus* gen. nov.,

23

sp nov., a marine, magnetotactic bacterium that represents a novel lineage (*Magnetococcaceae* fam. nov., *Magnetococcales* ord. nov.) at the base of the *Alphaproteobacteria*. Int J Syst Evol Microbiol **63**: 801-808.

Blakemore, R. P. (1975) Magnetotactic bacteria. Science **190**: 377-379.

Chang, L., Harrison, R. J., Zeng, F., Berndt, T. A., Roberts, A. P., Heslop, D. and Zhao, X. (2018) Coupled microbial bloom and oxygenation decline recorded by magnetofossils during the Palaeocene–Eocene Thermal Maximum. Nat Commun **9**: 4007.

Chang, S. B. R. and Kirschvink, J. L. (1989) Magnetofossils, the magnetization of sediments, and the evolution of magnetite biomineralization. Annu Rev Earth Planet Sci **17**: 169-195.

Chen, H., Li, J., Xing, X., Du, Z. and Chen, G. (2015) Unexpected diversity of magnetococci in intertidal sediments of Xiaoshi Island in the North Yellow Sea. J Nanomater **2015**: 902121.

Delong, E. F., Frankel, R. B. and Bazylinski, D. A. (1993) Multiple evolutionary origins of magnetotaxis in bacteria. Science **259**: 803-806.

Devouard, B., Pósfai, M., Hua, X., Bazylinski, D. A., Frankel, R. B. and Buseck, P. R. (1998) Magnetite from magnetotactic bacteria: size distributions and twinning. Am Mineral **83**: 1387-1398.

Egli, R. (2004) Characterization of individual rock magnetic components by analysis of remanence curves. 3. Bacterial magnetite and natural processes in lakes. Phys Chem Earth **29**: 869-884.

Esser, C., Martin, W. and Dagan, T. (2007) The origin of mitochondria in light of a fluid prokaryotic chromosome model. Biol Lett **3**: 180-184.

Flies, C. B., Jonkers, H. M., De Beer, D., Bosselmann, K., Böttcher, M. E. and Schüler, D. (2005a) Diversity and vertical distribution of magnetotactic bacteria along

24

chemical gradients in freshwater microcosms. FEMS Microbiol Ecol **52**: 185-195.

Flies, C. B., Peplies, J. and Schuler, D. (2005b) Combined approach for characterization of uncultivated magnetotactic bacteria from various aquatic environments. Appl Environ Microbiol **71**: 2723-2731.

He, K. and Pan, Y. X. (2020) Magnetofossil abundance and diversity as paleoenvironmental proxies: a case study from southwest Iberian margin sediments. Geophys Res Lett **47**: e2020GL087165.

Ji, B. Y., Zhang, S. D., Zhang, W. J., Rouy, Z., Alberto, F., Santini, C.-L., Mangenot, S., Gagnot, S.*, et al.* (2017) The chimeric nature of the genomes of marine magnetotactic coccoid-ovoid bacteria defines a novel group of *Proteobacteria*. Environ Microbiol **19**: 1103-1119.

Jovane, L., Florindo, F., Bazylinski, D. A. and Lins, U. (2012) Prismatic magnetite magnetosomes from cultivated Magnetovibrio blakemorei strain MV-1: a magnetic fingerprint in marine sediments? Environ Microbiol Rep **4**: 664-668.

Katzmann, E., Scheffel, A., Gruska, M., Plitzko, J. M. and Schüler, D. (2010) Loss of the actin‐like protein MamK has pleiotropic effects on magnetosome formation and chain assembly in *Magnetospirillum gryphiswaldense*. Mol Microbiol **77**: 208-224.

Kirschvink, J. L. and Chang, S. B. R. (1984) Ultrafine-grained magnetite in deep-sea sediments: possible bacterial magnetofossils. Geology **12**: 559-562.

Kobayashi, A., Kirschvink, J. L., Nash, C. Z., Kopp, R. E., Sauer, D. A., Bertani, L. E., Voorhout, W. F., and Taguchi, T. (2006), Experimental observation of magnetosome chain collapse in magnetotactic bacteria: sedimentological, paleomagnetic, and evolutionary implications. Earth Planet Sci Lett, **245**: 538-550.

25

Kolinko, S., Jogler, C., Katzmann, E., Wanner, G., Peplies, J. and Schüler, D. (2012) Single-cell analysis reveals a novel uncultivated magnetotactic bacterium within the candidate division OP3. Environ Microbiol **14**: 1709-1721.

Kolinko, S., Wanner, G., Katzmann, E., Kiemer, F., Fuchs, B. M. and Schüler, D. (2013) Clone libraries and single cell genome amplification reveal extended diversity of uncultivated magnetotactic bacteria from marine and freshwater environments. Environ Microbiol **15**: 1290-1301.

Komeili, A. (2012) Molecular mechanisms of compartmentalization and biomineralization in magnetotactic bacteria. FEMS Microbiol Rev **36**: 232-255.

Komeili, A., Vali, H., Beveridge, T. J. and Newman, D. K. (2004) Magnetosome vesicles are present before magnetite formation, and MamA is required for their activation. Proc Natl Acad Sci USA **101**: 3839-3844.

Kopp, R. E. and Kirschvink, J. L. (2008) The identification and biogeochemical interpretation of fossil magnetotactic bacteria. Earth-Sci Rev **86**: 42-61.

Koziaeva, V., Dziuba, M., Leão, P., Uzun, M., Krutkina, M. and Grouzdev, D. (2019) Genome-based metabolic reconstruction of a novel uncultivated freshwater magnetotactic coccus "*Ca.* Magnetaquicoccus inordinatus" UR-1, and proposal of a candidate Family "*Ca.* Magnetaquicoccaceae". Front Microbiol **10**: 2290.

Kozyaeva, V. V., Grouzdev, D. S., Dziuba, M. V., Kolganova, T. V. and Kuznetsov, B. B. (2017) Diversity of magnetotactic bacteria of the Moskva River. Microbiology **86**: 106-112.

Kumar, S., Stecher, G. and Tamura, K. (2016) MEGA7: molecular evolutionary genetics analysis version 7.0 for bigger datasets. Mol Biol Evol **33**: 1870-1874.

Lane, D. J. (1991) 16S/23S rRNA sequencing. In: Nucleic Acid Techniques in Bacterial Systematics. Wiley J. and Sons (ed), New York, pp. 115–175.

Larrasoaña, J. C., Liu, Q. S., Hu, P. X., Roberts, A. P., Mata, P., Civis, J., Sierro, F. J.

26

and Perez-Asensio, J. N. (2014) Paleomagnetic and paleoenvironmental implications of magnetofossil occurrences in late Miocene marine sediments from the Guadalquivir Basin, SW Spain. Front Microbiol **5**: 71.

Leão, P., Le Nagard, L., Yuan, H., Cypriano, J., Da Silva-Neto, I., Bazylinski, D. A., Acosta-Avalos, D., De Barros, H. L*., et al.* (2020) Magnetosome magnetite biomineralization in a flagellated protist: evidence for an early evolutionary origin for magnetoreception in eukaryotes. Environ Microbiol **22**: 1495-1506.

Lefèvre, C. T. and Bazylinski, D. A. (2013) Ecology, diversity, and evolution of magnetotactic bacteria. Microbiol Mol Biol Rev **77**: 497-526.

Lefèvre, C. T., Bernadac, A., Yu-Zhang, K., Pradel, N. and Wu, L. F. (2009) Isolation and characterization of a magnetotactic bacterial culture from the Mediterranean Sea. Environ Microbiol **11**: 1646-1657.

Lefèvre, C. T., Pósfai, M., Abreu, F., Lins, U., Frankel, R. B. and Bazylinski, D. A. (2011) Morphological features of elongated-anisotropic magnetosome crystals in magnetotactic bacteria of the *Nitrospirae phylum* and the *Deltaproteobacteria* class. Earth Planet Sci Lett **312**: 194-200.

Li, J. H., Benzerara, K., Bernard, S. and Beyssac, O. (2013a) The link between biomineralization and fossilization of bacteria: insights from field and experimental studies. Chem Geol **359**: 49-69.

Li, J. H., Ge, K. P., Pan, Y. X., Williams, W., Liu, Q. S. and Qin, H. F. (2013b) A strong angular dependence of magnetic properties of magnetosome chains: implications for rock magnetism and paleomagnetism. Geochem Geophys Geosyst **14**: 3887-3907.

Li, J. H., Menguy, N., Gatel, C., Boureau, V., Snoeck, E., Patriarche, G., Leroy, E. and Pan, Y. X. (2015) Crystal growth of bullet-shaped magnetite in magnetotactic bacteria of the *Nitrospirae* phylum. J R Soc Interface **12**: 20141288.

27

Li, J. H., Menguy, N., Roberts, A. P., Gu, L., Leroy, E., Bourgon, J., Yang, X. A., Zhao, X., Liu, P. Y., Changela, H., and Pan, Y. X. (2020), Bullet-shaped magnetite biomineralization within a magnetotactic Deltaproteobacterium: implications for magnetofossil identification, J Geophys Res-Biogeo, **125**: e2020JG005680.

Li, J. H., Zhang, H., Liu, P. Y., Menguy, N., Roberts, A. P., Chen, H. T., Wang, Y. Z. and Pan, Y. X. (2019) Phylogenetic and structural identification of a novel magnetotactic *Deltaproteobacteria* strain, WYHR-1, from a freshwater lake. Appl Environ Microbiol **85**: e00731-19.

Li, J. H., Zhang, H., Menguy, N., Benzerara, K., Wang, F. X., Lin, X. T., Chen, Z. B. and Pan, Y. X. (2017) Single-cell resolution of uncultured magnetotactic bacteria via fluorescence-coupled electron microscopy. Appl Environ Microbiol **83**: e00409-17.

Lin, W., Bazylinski, D.A., Xiao, T., Wu, L.-F., and Pan, Y.X. (2014) Life with compass: diversity and biogeography of magnetotactic bacteria. Environ Microbiol **16**: 2646-2658.

Lin, W., Kirschvink, J. L., Paterson, G. A., Bazylinski, D. A. and Pan, Y. X. (2019) On the origin of microbial magnetoreception. Natl Sci Rev **7**: 472-479.

Lin, W., Li, J. H., Schueler, D., Jogler, C. and Pan, Y. X. (2009) Diversity analysis of magnetotactic bacteria in Lake Miyun, northern China, by restriction fragment length polymorphism. Syst Appl Microbiol **32**: 342-350.

Lin, W. and Pan, Y. X. (2009) Uncultivated magnetotactic cocci from Yuandadu park in Beijing, China. Appl Environ Microbiol **75**: 4046-4052.

Lin, W. and Pan, Y. X. (2010) Temporal variation of magnetotactic bacterial communities in two freshwater sediment microcosms. FEMS Microbiol Lett **302**: 85-92.

Lin, W., Paterson, G. A., Zhu, Q. Y., Wang, Y. Z., Kopylova, E., Li, Y., Knight, R.,

Bazylinski, D. A., *et al.* (2017) Origin of microbial biomineralization and magnetotaxis during the Archean. Proc Natl Acad Sci USA **114**: 2171-2176.

Lin, W., Zhang, W. S., Zhao, X., Roberts, A. P., Paterson, G. A., Bazylinski, D. A. and Pan, Y. X. (2018) Genomic expansion of magnetotactic bacteria reveals an early common origin of magnetotaxis with lineage-specific evolution. ISME J **12**: 1508-1519.

Lins, U., McCartney, M. R., Farina, M., Frankel, R. B. and Buseck, P. R. (2006) Crystal habits and magnetic microstructures of magnetosomes in coccoid magnetotactic bacteria. An Acad Bras Ciênc **78**: 463-474.

Mann, S., Frankel, R. B. and Blakemore, R. P. (1984) Structure, morphology and crystal growth of bacterial magnetite. Nature **310**: 405-407.

Meldrum, F. C., Mann, S., Heywood, B. R., Frankel, R. B. and Bazylinski, D. A. (1993a) Electron microscopy study of magnetosomes in a cultured Coccoid magnetotactic bacterium. Proc R Soc Lond B **251**: 231-236.

Meldrum, F. C., Mann, S., Heywood, B. R., Frankel, R. B. and Bazylinski, D. A. (1993b) Electron microscopy study of magnetosomes in two cultured Vibrioid magnetotactic bacteria. Proc R Soc Lond B **251**: 237-242.

Monteil, C. L., Vallenet, D., Menguy, N., Benzerara, K., Barbe, V., Fouteau, S., Cruaud, C., Floriani, M., *et al.* (2019) Ectosymbiotic bacteria at the origin of magnetoreception in a marine protist. Nat Microbiol **4**: 1088-1095.

Morillo, V., Abreu, F., Araujo, A. C., De Almeida, L. G. P., Enrich-Prast, A., Farina, M., De Vasconcelos, A. T. R., Bazylinski, D. A. and Lins, U. (2014) Isolation, cultivation and genomic analysis of magnetosome biomineralization genes of a new genus of south-seeking magnetotactic cocci within the *Alphaproteobacteria*. Front Microbiol **5**: 72.

Murat, D., Quinlan, A., Vali, H. and Komeili, A. (2010) Comprehensive genetic

dissection of the magnetosome gene island reveals the step-wise assembly of a prokaryotic organelle. Proc Natl Acad Sci USA **107**: 5593-5598.

Muxworthy, A. R. and Williams, W. (2009) Critical superparamagnetic/single-domain grain sizes in interacting magnetite particles: implications for magnetosome crystals. J R Soc Interface **6**: 1207-1212.

Pan, H. M., Zhu, K. L., Song, T., Yu-Zhang, K., Lefèvre, C., Xing, S., Liu, M., Zhao, S. J.*, et al.* (2008) Characterization of a homogeneous taxonomic group of marine magnetotactic cocci within a low tide zone in the China Sea. Environ Microbiol **10**: 1158-1164.

Pósfai, M., Lefèvre, C. T., Trubitsyn, D., Bazylinski, D. A. and Frankel, R. B. (2013) Phylogenetic significance of composition and crystal morphology of magnetosome minerals. Front Microbiol **4**: 344.

Pósfai, M., Moskowitz, B. M., Arato, B., Schuler, D., Flies, C., Bazylinski, D. A. and Frankel, R. B. (2006) Properties of intracellular magnetite crystals produced by *Desulfovibrio magneticus* strain RS-1. Earth Planet Sci Lett **249**: 444-455.

Qian, X. X., Liu, J., Menguy, N., Li, J. H., Alberto, F., Teng, Z. J., Xiao, T., Zhang, W. Y. and Wu, L. F. (2019) Identification of novel species of marine magnetotactic bacteria affiliated with *Nitrospirae* phylum. Environ Microbiol Rep **11**: 330-337.

Qian, X. X., Santini, C. L., Kosta, A., Menguy, N., Le Guenno, H., Zhang, W. Y., Li, J. H., Chen, Y. R.*, et al.* (2020) Juxtaposed membranes underpin cellular adhesion and display unilateral cell division of multicellular magnetotactic prokaryotes. Environ Microbiol **22**: 1481-1494.

Roberts, A. P., Florindo, F., Villa, G., Chang, L., Jovane, L., Bohaty, S. M., Larrasoaña, J. C., Heslop, D. and Fitz Gerald, J. D. (2011) Magnetotactic bacterial abundance in pelagic marine environments is limited by organic carbon flux and

availability of dissolved iron. Earth Planet Sci Lett **310**: 441-452.

Rodelli, D., Jovane, L., Roberts, A. P., Cypriano, J., Abreu, F. and Lins, U. (2018) Fingerprints of partial oxidation of biogenic magnetite from cultivated and natural marine magnetotactic bacteria using synchrotron radiation. Environ Microbiol Rep **10**: 337-343.

Sakuramoto, Y., Yamazaki, T., Kimoto, K., Miyairi, Y., Kuroda, J., Yokoyama, Y. and Matsuzaki, H. (2017) A geomagnetic paleointensity record of 0.6 to 3.2 Ma from sediments in the western equatorial Pacific and remanent magnetization lock-in depth. J Geophys Res: Solid Earth **122**: 7525-7543.

Savian, J. F., Jovane, L., Frontalini, F., Trindade, R. I. F., Coccioni, R., Bohaty, S. M., Wilson, P. A., Florindo, F.*, et al.* (2014) Enhanced primary productivity and magnetotactic bacterial production in response to middle Eocene warming in the Neo-Tethys Ocean. Paleogeogr Paleoclimatol Paleoecol **414**: 32-45.

Savian, J. F., Jovane, L., Giorgioni, M., Iacoviello, F., Rodelli, D., Roberts, A. P., Chang, L., Florindo, F. and Sprovieri, M. (2016) Environmental magnetic implications of magnetofossil occurrence during the Middle Eocene Climatic Optimum (MECO) in pelagic sediments from the equatorial Indian Ocean. Paleogeogr Paleoclimatol Paleoecol **441**: 212-222.

Scheffel, A., Gardes, A., Grunberg, K., Wanner, G. and Schüler, D. (2008) The major magnetosome proteins MamGFDC are not essential for magnetite biomineralization in *Magnetospirillum gryphiswaldense* but regulate the size of magnetosome crystals. J Bacteriol **190**: 377-386.

Scheffel, A., Gruska, M., Faivre, D., Linaroudis, A., Plitzko, J. M. and Schüler, D. (2006) An acidic protein aligns magnetosomes along a filamentous structure in magnetotactic bacteria. Nature **440**: 110-114.

Schübbe, S., Williams, T. J., Xie, G., Kiss, H. E., Brettin, T. S., Martinez, D., Ross, C.

A., Schüler, D., *et al.* (2009) Complete genome sequence of the chemolithoautotrophic marine *Magnetotactic Coccus* strain MC-1. Appl Environ Microbiol **75**: 4835-4852.

Schüler, D. (2002) The biomineralization of magnetosomes in *Magnetospirillum gryphiswaldense*. Int Microbiol **5**: 209-214.

Singer, E., Emerson, D., Webb, E. A., Barco, R. A., Kuenen, J. G., Nelson, W. C., Chan, C. S., Comolli, L. R*., et al.* (2011) *Mariprofundus ferrooxydans* PV-1 the first genome of a marine Fe (II) oxidizing *Zetaproteobacterium*. PLoS One **6**: e25386.

Siponen, M. I., Legrand, P., Widdrat, M., Jones, S. R., Zhang, W.-J., Chang, M. C. Y., Faivre, D., Arnoux, P. and Pignol, D. (2013) Structural insight into magnetochrome-mediated magnetite biomineralization. Nature **502**: 681-684.

Spring, S., Amann, R., Ludwig, W., Schleifer, K. H. and Petersen, N. (1992) Phylogenetic diversity and identification of nonculturable magnetotactic bacteria. Syst Appl Microbiol **15**: 116-122.

Spring, S., Amann, R., Ludwig, W., Schleifer, K. H., Schüler, D., Poralla, K. and Petersen, N. (1995) Phylogenetic analysis of uncultured magnetotactic bacteria from the alpha-subclass of *Proteobacteria*. Syst Appl Microbiol **17**: 501-508.

Spring, S., Lins, U., Amann, R., Schleifer, K., Ferreira, L., Esquivel, D. and Farina, M. (1998) Phylogenetic affiliation and ultrastructure of uncultured magnetic bacteria with unusually large magnetosomes. Arch Microbiol **169**: 136-147.

Staniland, S. S. and Rawlings, A. E. (2016) Crystallizing the function of the magnetosome membrane mineralization protein Mms6. Biochem Soc Trans **44**: 883-890.

Tamura, K. and Nei, M. (1993) Estimation of the number of nucleotide substitutions in the control region of mitochondrial DNA in humans and chimpanzees. Mol Biol

32

Evol **10**: 512-526.

Toro-Nahuelpan, M., Giacomelli, G., Raschdorf, O., Borg, S., Plitzko, J. M., Bramkamp, M., Schüler, D. and Müller, F.-D. (2019) MamY is a membrane-bound protein that aligns magnetosomes and the motility axis of helical magnetotactic bacteria. Nat Microbiol **4**: 1978-1989.

Uebe, R. and Schüler, D. (2016) Magnetosome biogenesis in magnetotactic bacteria. Nat Rev Microbiol **14**: 621-637.

Usui, Y., Yamazaki, T. and Saitoh, M. (2017) Changing abundance of magnetofossil morphologies in pelagic red clay around Minamitorishima, western North Pacific. Geochem Geophys Geosyst **18**: 4558-4572.

Wang, Y. Z., Lin, W., Li, J. H. and Pan, Y. X. (2013) High diversity of magnetotactic *Deltaproteobacteria* in a freshwater niche. Appl Environ Microbiol **79**: 2813-2817.

Yamazaki, T. and Kawahata, H. (1998) Organic carbon flux controls the morphology of magnetofossils in marine sediments. Geology **26**: 1064-1066.

Yamazaki, T., Suzuki, Y., Kouduka, M. and Kawamura, N. (2019) Dependence of bacterial magnetosome morphology on chemical conditions in deep-sea sediments. Earth Planet Sci Lett **513**: 135-143.

Zhang, H., Menguy, N., Wang, F. X., Benzerara, K., Leroy, E., Liu, P. Y., Liu, W. Q., Wang, C. L.*, et al.* (2017) Magnetotactic coccus strain SHHC-1 affiliated to *Alphaproteobacteria* forms octahedral magnetite magnetosomes. Front Microbiol **8**: 969.

33

Figure and Table Captions

Figure 1. Phylogenetic and structural identification of representative magnetotactic cocci strains A-D. BHC-1, E-H. LLTC-1, I-L. DMHC-2, and M-P. MYC-3 using the coupled FISH-SEM approach. First column: fluorescence microscope maps (false colour) of bacteria hybridized by the 5′-FAM-labeled universal bacterial probe EUB338. Second column: fluorescence microscope maps (false colour) of bacteria hybridized by the 5′-Cy3-labeled species-specific probes. Third column: SEM images of the same area as in the first column. Forth column: high-magnification SEM image of targeted magnetotactic cocci marked by dashed boxes in the third column.

Figure 2. Phylogenetic position and morphology of magnetotactic cocci identified in this study. Blue background represents strains affiliated with the *Magnetococcales* order. A. Phylogenetic tree based on 16S rRNA gene sequences with the positions of magnetotactic cocci identified in this study in the *Magnetoccales* order. Bootstrap values at nodes are percentages of 1,000 replicates. The 16S rRNA gene sequence of the magnetotactic bacteria *Candidatus* Omnitrophus magneticus SKK-01 was used to root the tree. GenBank accession numbers are given in parentheses. B-U. TEM images of strains B. YQC-1, C. BHC-1, D. YQC-2, E. MYC-4, F. XJHC-1, G. LLTC-1, H. WYHC-2, I. SHHC-1, J. DMHC-1, K. WYHC-1, L. THC-1, M. MYC-5, N. DMHC-8, O. YQC-3, P. DMHC-2, Q. MYC-3, R. MYC-7, S. DMHC-6, T. WYCH-3, and U. SHHC-2. Strain SHHC-1 (indicated by the * symbol) was discovered in our previous study (Zhang *et al.*, 2017) from the same location as strain SHHC-2 and was used in this study for phylogenetic analysis and morphological comparison.

34

Figure 3. Cumulative probability distributions for magnetosomal magnetite length (first column), width (second column), and width to length ratio (axial ratio) (third column). The mean (colored solid line) and 95% confidence level (colored band) of each strain is estimated from 10,000 Monte Carlo simulations, which are further used to investigate the similarity of grain-size distributions of any two strains with a Kolmogorov-Smirnov test (Supplementary Material S2). A. Magnetotactic cocci with a single magnetite chain (for strains WHC-3, YQC-2, YQC-1, WYHC-1, and DMHC-1). B. Magnetotactic cocci with double chains (for strains YQC-3, XJHC-1, MYC-5, MYC-4, and LLTC-1). C. Magnetotactic cocci with two double chains (for strains DMHC-2, SHHC-1, and DMHC-8). D. Magnetotactic cocci with non-chain structure (for strains SHHC-2, DMHC-6, THC-1, MYC-7, WYHC-2, and MYC-3).

Figure 4. Phylogenetic distribution of MTB (black and red solid circles) and non-MTB (white empty circles) in the *Candidatus* Etaproteobacteria, *Alphaproteobacteria*, *Betaproteobacteria*, *Gammaproteobacteria*, *Deltaproteobacteria*, and *Epsilonproteobacteria* classes of the *Proteobacteria* phylum, the *Nitrospirae* phylum, and the *Candidatus* Omnitrophica phylum. Magnetotactic cocci strains identified in this study are marked by red solid circles.

Figure 5. Non-metric multidimensional scaling (nMDS) ordination plot of magnetosomal magnetite features (chain configuration, particle number, crystal width, and axial ratio) for magnetotactic cocci, using Euclidean distance and stress = 0.07. Data for individual cells of the same MTB species cluster together, while data for MTB species with the same chain configuration cluster in a small area.

35

Table 1. Morphological features of magnetotactic bacteria and their magnetosomal magnetite particles identified in this study.

Supplementary Figure S1. Chemical microanalysis of magnetosomes using STEM-EDX mapping in the high-angle annular dark-field (HAADF) mode. A. HAADF-STEM image of two MYC-4 cells and one unknown MTB cell, and corresponding chemical maps for B. C (C Kα), C. S (S Kα), and D. Fe (Fe Kα). E. RGB map with Fe (red), C (blue), and S (green). F. HAADF-STEM image of a DMHC-8 cell, and corresponding chemical maps of G. P (P Kα), H. S (S Kα), and I. Fe (Fe Kα). J. RGB map with Fe (red), P (blue), and S (green). K. EDX spectra for the carbon film covering the TEM grid (black), cell wall (indigo), magnetosomal magnetite particles (red), sulfur particle (green), and polyphosphate inclusion (blue).

Supplementary Figure S2. Morphological features of magnetosomal magnetite produced by six different magnetotactic cocci with a single chain configuration. TEM images of magnetite in strains A. BHC-1, B. YQC-1, C. YQC-2, D. WYHC-1, E. WYHC-3, and F. DMHC-1. Box-whisker plots of G. crystal length, H. width, and I. axial ratio of magnetite crystals, which reveal morphological differences among the strains.

Supplementary Figure S3. Morphological features of magnetosomal magnetite produced by five different magnetotactic cocci with a double chain configuration. TEM images of magnetite in strains A. MYC-4, B. MYC-5, C. YQC-3, D. LLTC-1, and E.

XJHC-1. Box-whisker plots of F. crystal length, G. width, and H. axial ratio of magnetite crystals, which reveal morphological differences among the strains.

Supplementary Figure S4. Morphological features of magnetosomal magnetite produced by three different magnetotactic cocci with two double chain configurations. TEM images of magnetite in strains A. DMHC-1, B. DMHC-8, and C. SHHC-1. Box-whisker plots of D. crystal length, E. width, and F. axial ratio of magnetite crystals, which reveal morphological differences among the strains. Strain SHHC-1 (indicated by the * symbol) was discovered in our previous study (Zhang *et al.*, 2017).

Supplementary Figure S5. Morphological features of magnetosomal magnetite produced by six different magnetotactic cocci with non-chain configuration. TEM images of magnetite in strains A. MYC-3, B. MYC-7, C. WYHC-2, D. THC-1, E. DMHC-6, and F. SHHC-2. Box-whisker plots of G. crystal length, H. width, and I. axial ratio of magnetite crystals, which reveal morphological differences among the strains.

Supplementary Figure S6. Grain size distribution of magnetite particles from magnetotactic cocci identified in this study. Boundaries between the single domain (SD), multi-domain (MD), and superparamagnetic (SP) regions are from Muxworthy and Williams (Muxworthy and Williams, 2009).

Supplementary Figure S7. Variability of morphological feature vectors for magnetite particles in magnetotactic cocci based on nMDS ordination results (9,999 permutations) by Envfit. The function of Envfit is fitting feature vectors or factors onto an ordination. The projections of points onto vectors have maximum correlation with corresponding

37

environmental variables, and the factors show the averages of factor levels. Clearly, the MDS1 axis principally represents crystal width, width/length ratio, and chain configuration, while the MDS2 axis principally represents the number of magnetite particles in the cell.

Supplementary Table S1. Sampling locations and environmental factors at the time of sampling.

Supplementary Table S2. FISH probes used in this study.

Supplementary Table S3. Mismatched information of FISH probes used in this study.

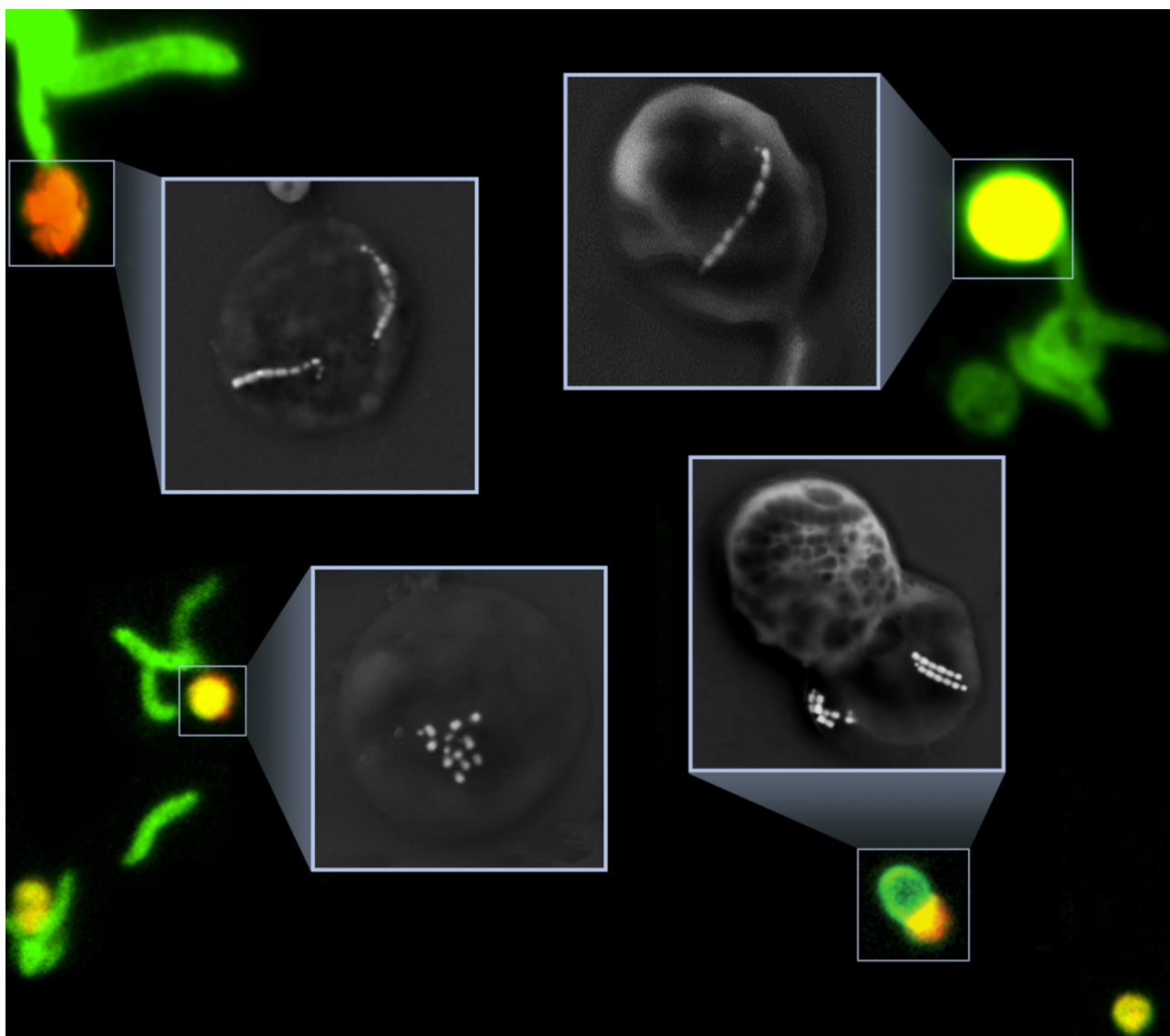**Supplementary Table S4.** 16S rRNA sequences retrieved from selected laboratory microcosms.

Supplementary Materials

Supplementary Material S1. Phylogenetic and structural identification of magnetotactic cocci using the coupled FISH-SEM approaches.
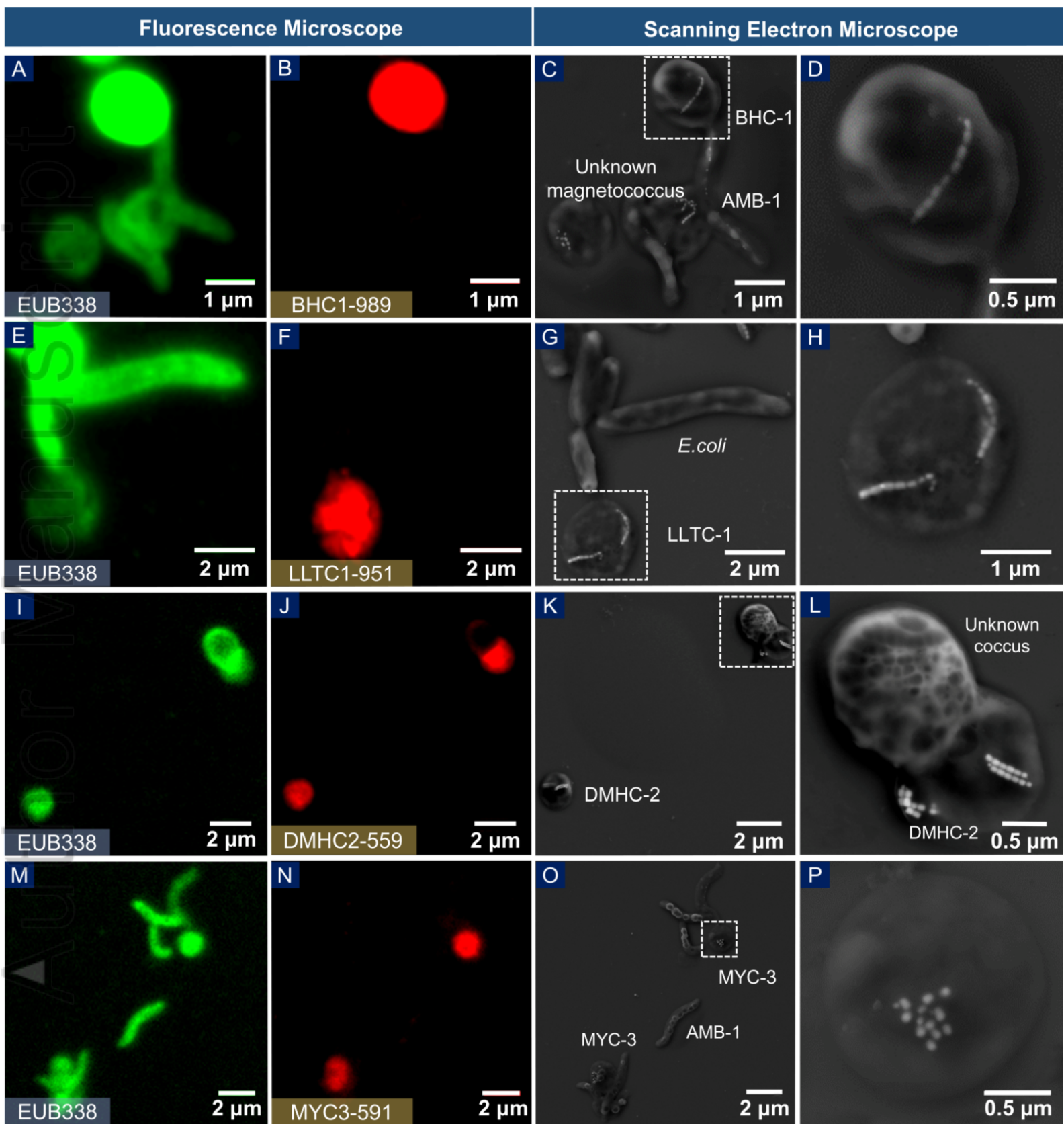
Supplementary Material S2. Two-samples Kolmogorov-Smirnov test of the length, width, and axial ratio of biogenic magnetite particles within magnetotactic cocci.

Supplementary Material S3. PERMANOVA results of magnetosomal magnetite biomineralization features (particle number, chain configuration, crystal width and width/length ratio) of 20 magnetotactic cocci strains by pairwise comparison. Strains marked in yellow represent MTB species with the same chain configuration. In contrast,
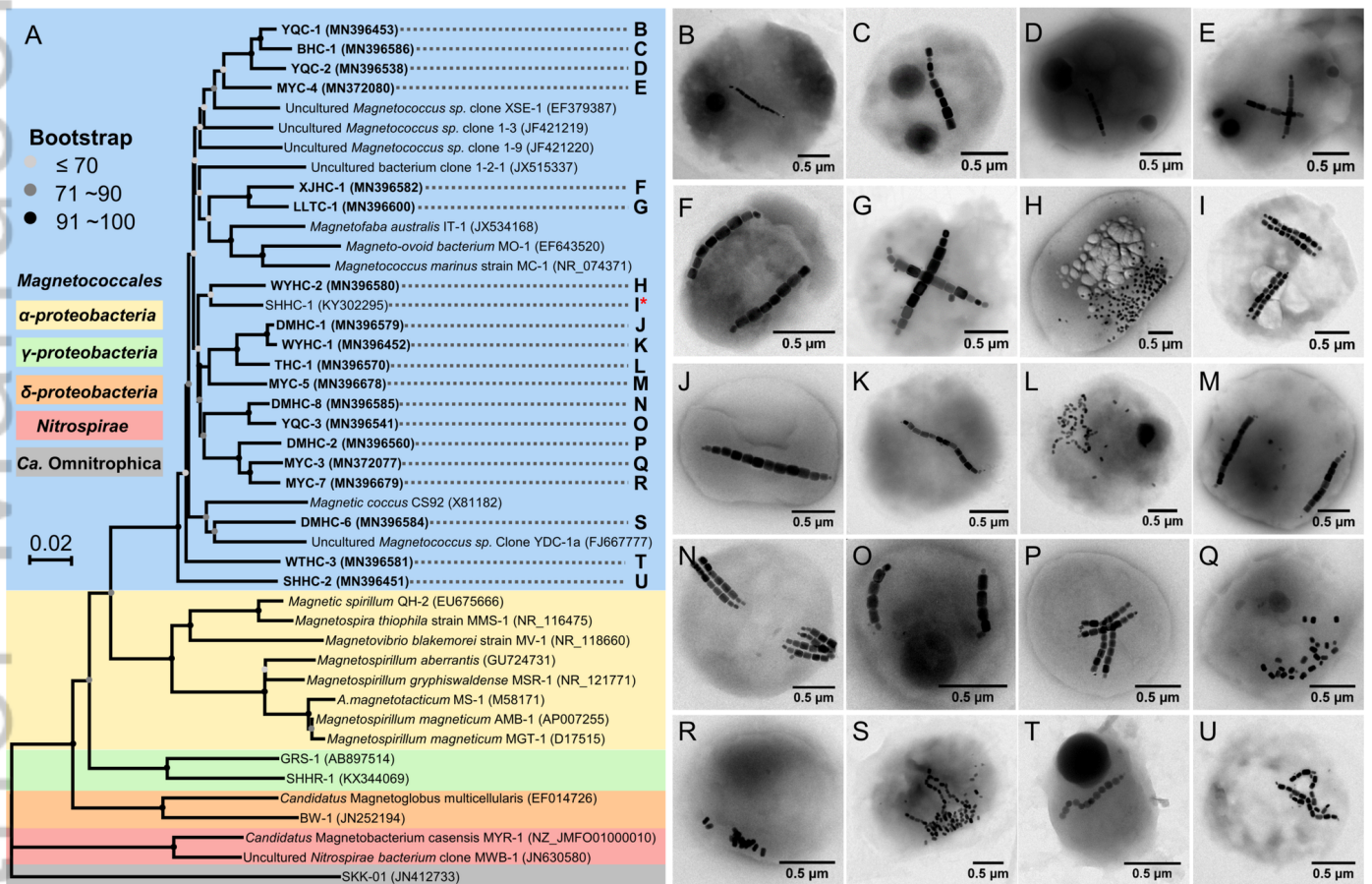
38

the others represent MTB species with different chain configurations. Group 1 and group 2 are the two comparison strains. Proportion of variance is the percentage of variance of the four biomineralization features.

EMI_15254_Cover image for EMI-2020-1220.R1.tif

Fluorescence Microscope

Scanning Electron Microscope

A — EUB338 — 1 µm

B — BHC1-989 — 1 µm

C — BHC-1, Unknown magnetococcus, AMB-1 — 1 µm

D — 0.5 µm

E — EUB338 — 2 µm

F — LLTC1-951 — 2 µm

G — E.coli, LLTC-1 — 2 µm

H — 1 µm

I — EUB338 — 2 µm

J — DMHC2-559 — 2 µm

K — DMHC-2 — 2 µm

L — Unknown coccus, DMHC-2 — 0.5 µm

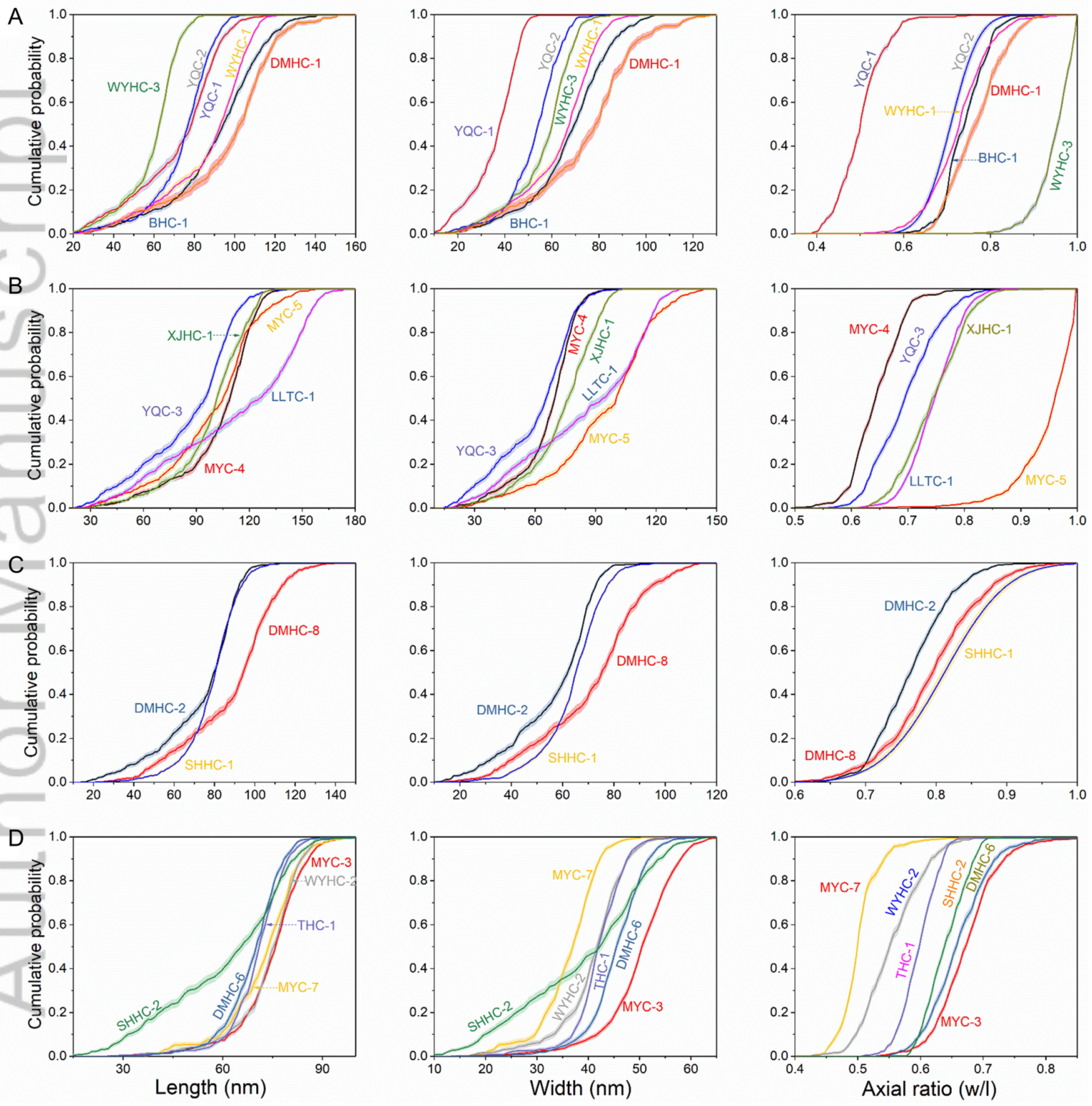M — EUB338 — 2 µm

N — MYC3-591 — 2 µm

O — MYC-3, MYC-3, AMB-1 — 2 µm

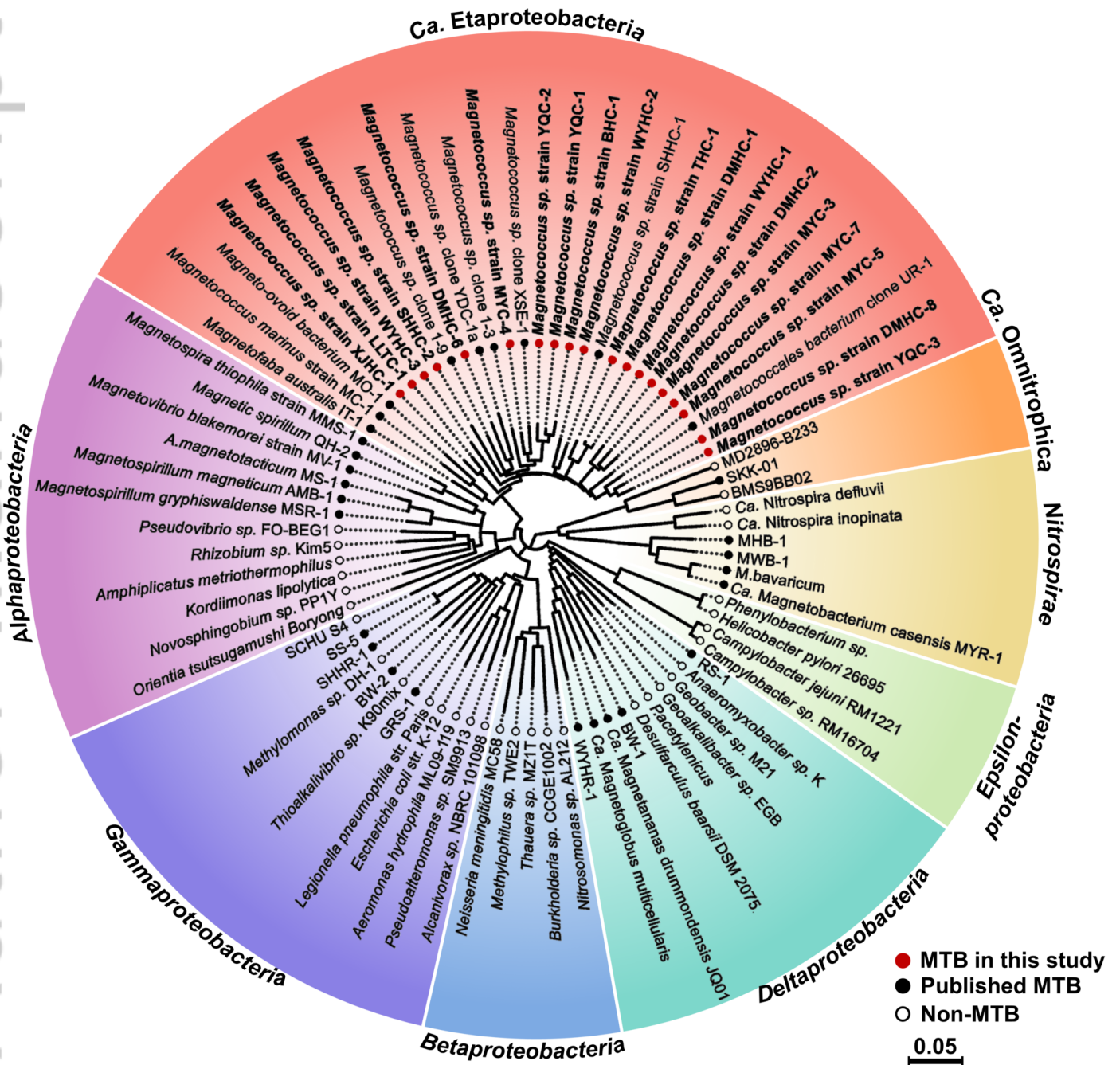P — 0.5 µm

EMI_15254_Figure 1.tif
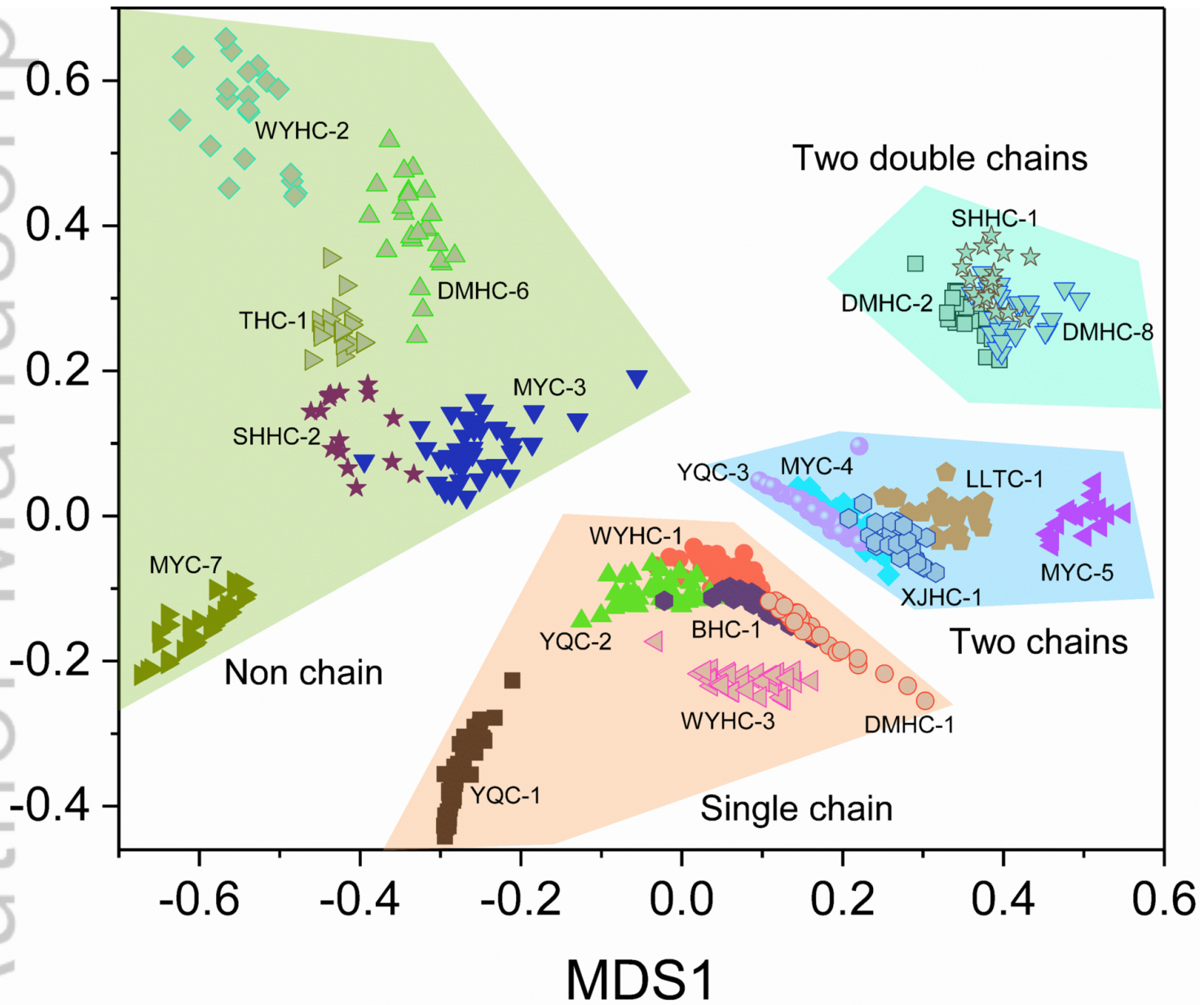
EMI_15254_Figure 2.tif

EMI_15254_Figure 3.tif

EMI_15254_Figure 4.tif

EMI_15254_Figure 5.tif

Diverse phylogeny and morphology of magnetite biomineralized by magnetotactic cocci

Peiyu Liu,[1,2,3,4] Yan Liu,[1,2,3,4] Xiang Zhao,[5] Andrew P. Roberts,[5] Heng Zhang,[1,2] Yue Zheng,[6] Fuxian Wang,[1,2,3,4] Lushan Wang,[7] Nicolas Menguy,[4,8] Yongxin Pan,[1,3,4] Jinhua Li[1,2,4*]

[1]Key Laboratory of Earth and Planetary Physics, Institute of Geology and Geophysics, Innovation Academy for Earth Science, Chinese Academy of Sciences, Beijing 100029, China

[2]Laboratory for Marine Geology, Qingdao National Laboratory for Marine Science and Technology, Qingdao 266061, China

[3]College of Earth and Planetary Sciences, University of Chinese Academy of Sciences, Beijing 100049, China

[4]France-China Joint Laboratory for Evolution and Development of Magnetotactic MultiCellular Organisms, Chinese Academy of Sciences, Beijing 100029, China

[5]Research School of Earth Sciences, Australian National University, Canberra, ACT 2601, Australia

[6]Key Laboratory of Urban Pollutant Conversion, Institute of Urban Environment, Chinese Academy of Sciences, Xiamen 361021, China

[7]State Key Laboratory of Microbial Technology, School of Life Sciences, Shandong University, Qingdao 266237, China

[8]IMPMC, CNRS UMR 7590, Sorbonne Universités, MNHN, UPMC, IRD UMR 206, 75005 Paris, France

*For correspondence. E-mail: lijinhua@mail.iggcas.ac.cn; Tel. (+86) 10 82998323; Fax (+86) 10 62010846

Conflict of interest. The authors declare that they have no conflict of interest.

Running title. Diversity and biomineralization of MTB

1

Abstract. Magnetotactic bacteria (MTB) are diverse prokaryotes that produce magnetic nanocrystals within intracellular membranes (magnetosomes). Here, we present a large-scale analysis of diversity and magnetosome biomineralization in modern magnetotactic cocci, which are the most abundant MTB morphotypes in nature. Nineteen novel magnetotactic cocci species are identified phylogenetically and structurally at the single-cell level. Phylogenetic analysis demonstrates that the cocci cluster into an independent branch from other *Alphaproteobacteria* MTB, i.e., within the *Etaproteobacteria* class in the *Proteobacteria* phylum. Statistical analysis reveals species-specific biomineralization of magnetosomal magnetite morphologies. This further confirms that magnetosome biomineralization is controlled strictly by the MTB cell and differs among species or strains. The post-mortem remains of MTB are often preserved as magnetofossils within sediments or sedimentary rocks, yet paleobiological and geological interpretation of their fossil record remains challenging. Our results indicate that magnetofossil morphology could be a promising proxy for retrieving paleobiological information about ancient MTB.

Summary. Magnetotactic bacteria (MTB) could be the earliest organisms with geomagnetic field-sensing and biomineralizing capability on Earth. Understanding the microbial diversity and biomineralization products of modern MTB is fundamental to developing paleoecological, paleobiological, and paleoenvironmental proxies of their fossil record. Identification of ancient magnetofossils is challenging because the link between microbial phylogeny and biomineralization is not well documented. We

2

present a large-scale analysis that combines microbial phylogenesis and nanoscale mineral characterization to demonstrate a robust relationship between species and morphology of biomineralized magnetite within magnetotactic bacteria. Experimental results provide evidence that magnetosome biomineralization differs among different species or strains. Therefore, magnetofossil morphology is likely to be a promising proxy for retrieving paleobiological information from ancient MTB.

Introduction

Magnetotactic bacteria (MTB) have long been of interest to biologists and geologists because they could represent the earliest geomagnetic field-sensing organisms on Earth (Kopp and Kirschvink, 2008; Uebe and Schüler, 2016; Lin *et al.*, 2017). They are morphologically and phylogenetically diverse prokaryotes that produce intracellularly size-tailored and morphologically-defined nanocrystals of magnetite (Fe_3O_4) or/and greigite (Fe_3S_4) each enveloped by a lipid bilayer membrane called a magnetosome (Bazylinski and Frankel, 2004; Lefèvre and Bazylinski, 2013). Fossil remains of these biominerals (magnetofossils) have been reported widely from Cenozoic sedimentary environments and have been used to retrieve paleomagnetic and tentative paleoenvironmental information (Kirschvink and Chang, 1984; Chang and Kirschvink, 1989; Kopp and Kirschvink, 2008; Roberts *et al.*, 2011; Larrasoaña *et al.*, 2014; Savian *et al.*, 2014; Savian *et al.*, 2016; Sakuramoto *et al.*, 2017; Chang *et al.*, 2018). Studying the biodiversity and biomineralization of MTB is crucial to understand the evolution of iron mineral-based magnetoreception within higher organisms (Lins *et al.*, 2006; Lin *et al.*, 2018; Lin *et al.*, 2019; Monteil *et al.*, 2019; Leão *et al.*, 2020). Such studies also provide the principal information needed to develop magnetofossils as novel biogeochemical proxies for simultaneous paleomagnetic, paleoenvironmental,

3

and paleobiological reconstructions (Kopp and Kirschvink, 2008; Jovane *et al.*, 2012; Li *et al.*, 2013a; Rodelli *et al.*, 2018; Yamazaki *et al.*, 2019; Li *et al.*, 2020).

Coccoid-to-ovoid MTB, the so-called magnetotactic cocci, are the most commonly observed morphotypes in natural environments. However, few have been identified and studied, possibly due to the fact that they are fastidious with respect to growth and difficult to distinguish based on their bacterial morphology. So far, only three magnetotactic cocci from marine environments have been cultured axenically: *Magnetococcus marinus* strain MC-1 (Bazylinski *et al.*, 2013), strain MO-1 (Lefèvre *et al.*, 2009), and *Magnetofaba australis* strain IT-1 (Morillo *et al.*, 2014). In addition, despite retrieval of a large number of 16S rRNA gene sequences potentially affiliated with magnetotactic cocci from various environmental samples (Spring *et al.*, 1995; 1998; Lin and Pan, 2009; Kozyaeva *et al.*, 2017; Lin *et al.*, 2018), only a few have been linked unambiguously to a single MTB morphotype (Pan *et al.*, 2008; Lin and Pan, 2009; Kolinko *et al.*, 2013; Abreu *et al.*, 2016; Koziaeva *et al.*, 2019). The missing link between bacterial phylogeny and magnetic nanoparticle structure and chain arrangement at the single-cell level (Li *et al.*, 2017; Zhang *et al.*, 2017) hinders understanding of bacterial taxonomy and biomineralization within magnetotactic cocci.

In this study, 19 novel magnetotactic cocci strains from varied freshwater, brackish, and marine environments were identified phylogenetically and structurally using a coupled fluorescence *in situ* hybridization (FISH) and scanning electron microscope (SEM) method developed for single-cell analysis (Li *et al.*, 2017). Together with strain SHHC-1 identified by our group in a previous study (Zhang et al., 2017), the number, size, and morphology of magnetite particles and their chain assembly within these 20 magnetotactic cocci were then determined from detailed transmission electron microscope (TEM) observations. Finally, the relationship between biomineralization

4

and bacterial phylogeny is analyzed statistically. Our large-scale identification of novel magnetotactic cocci strains supports strongly the suggestion that magnetotactic cocci should be reclassified into an independent class in the *Proteobacteria* phylum (Ji *et al.*, 2017; Lin *et al.*, 2018). Our results also test and validate, with the largest assessment available so far, the assumption of species-specific control of magnetosomal magnetite biomineralization within MTB, which provides a foundation for using magnetofossil morphology as a proxy for paleoecological and paleoenvironmental reconstructions.

Results

Bacterial identification and phylogenetic analysis

Fourteen laboratory microcosms dominated by magnetotactic cocci were selected for magnetic enrichment of living MTB cells. According to molecular analyses of 16S rRNA gene sequencing, most cells (79.8%) retrieved from the magnetic enrichments were identified as magnetotactic cocci, along with other MTB and non-MTB types that accounted for 13.3% and 6.9% of cells, respectively (Table S4). Specifically, magnetic enrichments from two microcosms likely contain only one magnetotactic coccus type based on 16S rRNA gene sequence analyses. They were collected from Shihe Estuary (Microcosm-12) and Laolongtou Bay (Microscosm-14). Both are dominant by coastal sandy sediments. In contrast, the other twelve microcosms are dominant by argillaceous sediments due to that they were collected from one tidal flat environment (Microscosm-13) and lake or river environments (Microcosms 1-11) (Table S1). They contain diverse MTB (magnetotactic cocci and other MTB types) and non-MTB species (Table S4). This result indicates a general coexistence of phylogenetically diverse MTB in nature. It also indicates that the widely used method of magnetic separation of MTB from sediments does not avoid contamination by non-MTB cells. Therefore, considering the

5

generally complex composition of MTB in nature or laboratory microcosms, it is necessary to link a targeted 16S rRNA gene to a specific MTB morphotype at single-cell scale. With the help of the recently-developed coupled FISH-SEM approach (Li *et al.*, 2017), we then identified 19 types of magnetotactic cocci from these 14 enriched samples.

As shown in Figure 1, targeted MTB were hybridized with both the EUB338 universal bacterial probe (green) and the corresponding species-specific MTB probe (red), while others (including other types of MTB, non-MTB, and inner control cells of *E. coli* or *Magneospirillum magneticum* AMB-1) were only hybridized with the EUB338 probe. Subsequent coordinated SEM observations on the fluorescence-labeled bacteria further reveal the detailed morphological and structural features of both cells and their intracellular magnetosomes. With this strategy, we identified 16 magnetotactic cocci from freshwater environments (strains YQC-1, YQC-2, YQC-3, THC-1, BHC-1, MYC-3, MYC-4, MYC-5, MYC-7, DMHC-1, DMHC-2, DMHC-6, DMHC-8, WYHC-1, WYHC-2, and WYHC-3), two from marine environments (strains XJHC-1 and LLTC-1), and one from a brackish environment (strain SHHC-2). Based on FISH-SEM analyses, the cells identified here can be classified into four groups according to their magnetosome chain configuration: single chain, double-separated chains, double parallel chains, and particle aggregates (Figure 1). Careful observations on more target cells demonstrated that for all the cells hybridized by one species-specific oligonucleotide probe contain magnetosomes with identical chain arrangement (Supplementary material S1).

Phylogenetic analysis from 16S rRNA gene sequences indicate that all 19 magnetotactic cocci have a common sequence identity lower than 97%, so they can be assembled as different species in the phylogenetic tree (Fig. 2A). Further sequence

6

alignment reveals that eight of the magnetotactic cocci (strains MYC-3, MYC-7, DMHC-1, DMHC-8, YQC-1, YQC-3, THC-1, and LLTC-1) have high similarity (97-99% for different strains) to previously known 16S rRNA sequences (Table 1) (Spring *et al.*, 1998; Flies *et al.*, 2005b; Lin *et al.*, 2009; Lin and Pan, 2010; Wang *et al.*, 2013; Chen *et al.*, 2015). The other 11 magnetotactic cocci may represent novel species due to sequence identities lower than 97% with respect to known sequences. TEM observation was carried out following the coupled FISH-SEM analyses. Phylogenic tree and representative TEM images of all 19 magnetotactic cocci are shown in Figure 2.

Chemical and morphological characterization

TEM observations reveal that most of the magnetotactic cocci have spherical morphologies except for a few ovoid cocci (e.g., WYHC-2 (Fig. 2H) and DMHC-1 (Fig. 2J)), with average sizes ranging from ~1.0 to ~2.5 µm. Most magnetotactic cocci contain more than 10 magnetite particles per cell. In contrast, strains DMHC-6 (Fig. 2S) and WYHC-2 (Fig. 2H) produce relatively more magnetosomal particles, i.e., averages of 70±13 and 103±16 particles per cell, respectively (Table 1). Energy dispersive X-ray (EDX) spectroscopy coupled with scanning TEM (STEM) observations demonstrate that these particles are rich in iron and oxygen, which indicates that the studied magnetotactic cocci biomineralize magnetosomal magnetite crystals (Fig. S1).

The chain configuration and crystal morphology of magnetosomes within each MTB species were investigated in detail by TEM observations (Fig. 2, Table 1). Magnetite particles are arranged into a single chain in strains YQC-1, BHC-1, YQC-2, DMHC-1, WYHC-1, and WYHC-3 (Fig. 2B-D, J, K, T), whereas double separated chains occur in strains MYC-4, XJHC-1, LLTC-1, MYC-5, and YQC-3 (Fig. 2E-G, M, O), and two double chains occur in strains DMHC-8 and DMHC-2 (Fig. 2N, P).

7

Magnetite particles within the other six strains are not arranged into linear single or multiple chains and consist of dispersed aggregates (strains WYHC-2, THC-1, MYC-3, and MYC-7; Fig. 2H, L, Q, R), dispersed aggregates and partial chains (strain DMHC-6; Fig. 2S), and particle clusters and partial chains (strain SHHC-2; Fig. 2U). Despite having nearly identical chain configuration in all cells for each MTB species, there is no obvious correlation between the phylogenetic relatedness and the chain arrangement. This indicates that the chain configuration of magnetosomes is important but not unique feature for distinguishing different MTB.

Most of the studied magnetotactic cocci strains produce elongated prismatic projections with axial ratio (i.e., width/length) values lower than 0.8, except for strains MYC-5 and WYHC-3, which produce octahedral and cubo-octahedral magnetite morphologies, respectively (Figs. S2-S5). Strain DMHC-2 appears to form elongated cubo-octahedral magnetite crystals (Figure S4). Our previous study has shown that strain SHHC-1 forms elongated octahedral magnetite crystals (Zhang *et al.*, 2017). Nevertheless, crystal sizes and their axial ratios are different (Table 1). Statistically, each strain appears to produce magnetite particles with their own crystal size and shape distributions (Fig. 3). A two-dimensional Kolmogorov–Smirnov test confirms that the magnetite morphologies are statistically different among the magnetotactic cocci (Supplementary material S2).

Despite their structural and morphological diversity, magnetite particles produced by these magnetotactic cocci share common features, as observed in other cultured and uncultured MTB that produce prismatic, octahedral, or cubo-octahedral magnetite particles (Devouard *et al.*, 1998; Li *et al.*, 2013b; Pósfai *et al.*, 2013). For instance, structural and morphological features of magnetite within the same magnetotactic coccus strain are uniform, i.e., identical chain configuration and narrow particle number

8

distribution (Fig. 3, Figs. S2-S5). Crystal length and width distributions are all skewed negatively with skewness values ranging from -0.57 to -1.47 for length and from -0.44 to -1.34 for width. In addition, the magnetite crystals have relatively narrow size distributions with average lengths ranging from ~60 to ~114 nm and an average width from ~36 to 86 nm, which fall within the magnetically ideal size range for stable single domain (SD) particles (Fig. S6) (Muxworthy and Williams, 2009). These observations confirm that chain configurations and crystal morphologies are diverse in MTB, but that they are homogeneous for a given MTB species or strain (Pósfai *et al.*, 2013).

Notably, magnetotactic cocci appear to organize their magnetosomal magnetite particles in a relatively more complicated way compared to other MTB (e.g., Kobayashi *et al.*, 2006). The spatial arrangement of magnetite magnetosomes within magnetotactic cocci, particularly with non-chain structure and corresponding molecular mechanisms, deserve further study by electron tomography and comparative genomics (e.g., Zhang *et al.*, 2017; Lin *et al.*, 2018). In addition, consistent with previous studies (Mann *et al.*, 1984; Meldrum *et al.*, 1993a, Meldrum *et al.*, 1993b; Li *et al.*, 2013b; Li *et al.*, 2017; Zhang *et al.*, 2017), small (immature) magnetite particles are often observed at the ends of magnetosome chains within most magnetotactic cocci. However, tiny magnetite particles can also be distributed outside magnetosome chains within strain LLTC-1, resulting in a particularly long tail with smaller length and width distributions (Fig. 3B). This may suggest that magnetic particles within strain LLTC-1 grow gradually.

Discussion and conclusions

Diversity and taxonomic position of magnetotactic cocci

The taxonomic position of magnetotactic cocci has long been debated, despite their widespread detection in natural environments since the mid-1970s (Blakemore, 1975;

9

Lefèvre and Bazylinski, 2013). Early cultivation-independent studies based on phylogenetic analysis of 16S rRNA genes proposed that magnetotactic cocci are affiliated within the *Alphaproteobacteria*, but that they form a separate lineage (Spring *et al.*, 1992; Delong *et al.*, 1993; Spring *et al.*, 1995; Spring *et al.*, 1998; Flies *et al.*, 2005a), or represent the earliest-diverging *Alphaproteobacteria* branch (Esser *et al.*, 2007; Bazylinski *et al.*, 2013). Conversely, one early study suggested that *Magnetococcus marinus* MC-1 should be assigned to a novel *Proteobacteria* subdivision because it appears to be related more closely to the class *Zetaproteobacteria* based on a phylogenetic tree of 16S rRNA genes (Singer *et al.*, 2011). From comparative genomic and metagenomic studies of both cultured and uncultured MTB, two recent studies further proposed that magnetotactic cocci might represent a novel monophyletic class of *Proteobacteria* (i.e., "*Candidatus* Etaproteobacteria") (Ji *et al.*, 2017; Lin *et al.*, 2018). However, most investigators insist that magnetotactic cocci should be clustered into a new order *Magnetococcales*, which represents the basal-most lineage within the *Alphaproteobacteria*, because the overall topologies of these phylogenetic trees are based on a limited number of data that preclude definitive determination of the taxonomic position of magnetotactic cocci (Bazylinski *et al.*, 2013; Lefèvre and Bazylinski, 2013).

The three axenically cultured magnetotactic cocci strains all produce a few to a dozen magnetite particles that are arranged into a single intracellular chain (Lefèvre *et al.*, 2009; Bazylinski *et al.*, 2013; Morillo *et al.*, 2014). Magnetotactic cocci are generally small and spherical or ovoid. They are not easy to identify unambiguously using traditional molecular ecology techniques and fluorescence microscopy (Li *et al.*, 2017). Our FISH-SEM approach couples fluorescence and electron microscope observations on the same bacteria targeted with fluorescently labelled oligonucleotide

10

probes, and has proven to be practicable for single-cell phylogenetic and structural identification of uncultivated MTB from complex and diverse microbial communities in environmental samples (Li *et al.*, 2017; Zhang *et al.*, 2017; Li *et al.*, 2019; Qian *et al.*, 2019; Qian *et al.*, 2020). This study is the first to identify and analyze large numbers of magnetotactic cocci from varied aquatic environments using the coupled FISH-SEM method and TEM characterization. Our results provide substantial evidence to better understand bacterial diversity and the taxonomic position of magnetotactic cocci, as well as magnetite biomineralization within them. As shown in Figure 4, phylogenetic analyses based on 16S rRNA gene sequences indicate that all 19 identified strains cluster into an independent phylogenetic branch along with several previously reported magnetotactic cocci, which are related distantly to the *Alphaproteobacteria*, *Gammaproteobacteria, Betaproteobacteria*, *Deltaproteobacteria*, and *Epsilonproteobacteria* in the *Proteobacteria* phylum.

Different from morphologically diverse MTB within other classes or phyla, all bacteria affiliated with the *Etaproteobacteria* identified so far have spherical or ovoid cell morphologies. Also different from the co-classification of non-MTB and MTB within other classes or phyla, the bacteria discovered so far from the *Etaproteobacteria* class are all MTB (Fig. 4). This suggests that the *Etaproteobacteria* might consist only of magnetotactic cocci. One interpretation of this observation is that the magnetosome gene cluster (MGC, i.e., the genes responsible for magnetosomal biomineralization) within magnetotactic cocci is more stable than in other MTB due to a lack of transposable elements around or within the MGC (Schübbe *et al.*, 2009; Morillo *et al.*, 2014; Ji *et al.*, 2017; Lin *et al.*, 2018). Alternatively, it is possible that non-MTB species affiliated with the *Etaproteobacteria* class exist in natural environments, which needs more extensive survey. In addition, comparative genomic analysis reveals that the

11

genomes of magnetotactic cocci strains MC-1 and MO-1 have a mosaic origin affiliated with *Alphaproteobacteria*, *Betaproteobacteria*, *Gammaproteobacteria*, *Deltaproteobacteria*, or *Epsilonproteobacteria* (Ji *et al.*, 2017). This suggests that the *Etaproteobacteria* class may represent a transition between the *Deltaproteobacteria* and the *Alphaproteobacteria*, *Betaproteobacteria*, *Gammaproteobacteria*, or even an ancestor of the *Proteobacteria* phylum. Further genomic analyses on the uncultured magnetotactic cocci identified here will provide more clues to better understand the origin and evolution of MTB and of magnetoreception within MTB.

Relationship between magnetite biomineralization and bacterial phylogeny

Our study demonstrates that magnetosomal magnetite biomineralization (e.g., chain configuration, particle number, crystal size, and morphology) within magnetotactic cocci is diverse (Fig. 2, Table 1). To understand the relationship between magnetite biomineralization and MTB species, non-metric multidimensional scaling (nMDS) analysis was carried out on four main aspects, including chain configuration, particle number, crystal width, and axial ratio (Fig. S7). As shown in Figure 5, nMDS analysis indicates that data for all cells from the same MTB species tend to gather together in the nMDS plot, and that data for different MTB species are relatively dispersed from each other. Permutational multivariate analysis (PERMANOVA) based on the nMDS results further reveals that the difference in magnetite biomineralization between two random MTB species is significant (P<0.001, Supplementary material S3).

The nature of chain configurations contributes dominantly to the nMDS results for all MTB species with proportion of variance up to ~84%, so that MTB species with the same chain configuration cluster into a separate region from others (Fig. 5). For MTB species with no chains, the number of magnetite particles per cell contributes

12

dominantly with proportion of variance up to ~84%. For the three other chain configurations, crystal width or axial ratio provide a primary contribution with proportion of variance up to ~61% (Supplementary material S3). It has been demonstrated that biomineralization within MTB is strictly controlled genetically, and that features such as chain arrangement, particle number, crystal size, and morphology are related directly or indirectly to certain genes within its MGC (Murat *et al.*, 2010; Komeili, 2012; Uebe and Schüler, 2016). The *mamK*, *mamJ*, and *mamY* genes are responsible for chain construction within magnetotactic spirilla (strains AMB-1 and MSR-1) (Scheffel *et al.*, 2006; Katzmann *et al.*, 2010; Toro-Nahuelpan *et al.*, 2019). The *mamC*, *mamD*, *mamG*, *mamF*, and *mms6* genes are related to crystal size and morphology (Scheffel *et al.*, 2008; Staniland and Rawlings, 2016), while *mamA*, *mamP*, mam*T*, and *mamS* are associated with the number of particles (Komeili *et al.*, 2004; Murat *et al.*, 2010; Siponen *et al.*, 2013; Uebe and Schüler, 2016). In contrast to *Magnetospirilla*, only several core genes (mamABFKMOPI) are observed on the MGCs of three cultured magnetotactic cocci (strains MC-1, MO-1, and IT-1) and one uncultured strain (*Ca.* Magnetaquicoccus inordinatus UR-1) (Schübbe *et al.*, 2009; Morillo *et al.*, 2014; Ji *et al.*, 2017; Koziaeva *et al.*, 2019). Therefore, the copy number variation and divergence of these core genes or/and other unknown genes in the MGCs of different MTB species may result in diverse biomineralization within magnetotactic cocci, which also needs further genomic study.

Direct analysis of magnetofossil morphology in the ancient sedimentary record is being used increasingly to reconstruct paleoenvironments (Yamazaki and Kawahata, 1998; Egli, 2004; Usui *et al.*, 2017; Chang *et al.*, 2018; Yamazaki *et al.*, 2019; He and Pan, 2020). Yamazaki and Kawahata (1998) found that magnetofossils in Pacific deep-sea sediments are more isotropic in more oxidizing paleo-conditions and are more

13

anisotropic in more reducing environments. Chang *et al.* (2018) reconstructed a deep-sea ecological pattern of coupled MTB increases with an oxygenation decline during the Paleocene–Eocene Thermal Maximum (PETM) through quantifying magnetofossil abundance and morphology from the PETM onset to its peak at Walvis Ridge, South Atlantic Ocean. Studies of modern MTB indicate that the distribution, presence, and abundance of MTB are affected by environmental parameters such as salinity, oxygen, temperature, or sulfur compounds (e.g., Lin *et al.*, 2014). The crystal morphology of biogenic magnetite is associated with MTB phylogenetic group (Pósfai *et al.*, 2013). For example, MTB affiliated with *Etaproteobacteria*, *Alphaproteobacteria*, and *Gammaproteobacteria* produce magnetosomal magnetite with octahedral, cubo-octahedral, or elongated prismatic shapes (Mann *et al.*, 1984; Meldrum *et al.*, 1993a, Meldrum *et al.*,1993b; Li *et al.*, 2013b; Li *et al.*, 2017; Zhang *et al.*, 2017), while MTB in the class *Deltaproteobacteria*, *Nitrospirae*, and *Omnitrophica* produce highly elongated anisotropic magnetite crystals (Pósfai *et al.*, 2006; Lefèvre *et al.*, 2011; Kolinko *et al.*, 2012; Li *et al.*, 2015; Li *et al*., 2020). Our results further demonstrate that a combination of physical features (i.e., chain configuration, particle number, crystal morphology, and size) can distinguish MTB groups even at species or strain level. This indicates that comprehensive analysis of chain assembly, particle number, crystal morphology, and size should provide a robust basis for MTB classification and magnetofossil identification. To do this, systematic study of the relationship between bacterial phylogeny, magnetite biomineralization, and environmental factors (e.g., salinity, oxygen, temperature, and pH) in modern MTB is required urgently to develop the use of magnetofossils as a biogeochemical proxy, i.e., to retrieve information about the environments in which ancient MTB lived. In concert, larger scale studies of MTB in various environments are needed to develop a much more extensive database of

14

phylogenetic information coupled with nanoscale characterization of physical aspects of the magnetite biomineralized by MTB.

In summary, we present a large-scale bacterial characterization of magnetosomal magnetite from wild-type magnetotactic cocci. In total, 19 novel strains were identified phylogenetically and structurally for the first time using a coupled FISH-SEM approach at the single-cell level. Phylogenetic analysis demonstrates that these strains cluster into an independent branch from other *Alphaproteobacteria* MTB, which supports strongly the idea that the order *Magnetococcales* should become a new class, i.e., the *Etaproteobacteria* class in the *Proteobacteria* phylum (Ji *et al.*, 2017; Lin *et al.*, 2018). Systematic TEM observations demonstrate diverse magnetite biomineralization among magnetotactic cocci strains in terms of particle number, crystal size, axial ratio, and chain configuration, whereas these variables are generally homogeneous for a given species. Statistical analysis between bacterial phylogeny and magnetite biomineralization further reveals species-specific biomineralization, which indicates that magnetite production is controlled strictly by the MTB cell with different morphologies produced by different species or strains. Further extensive studies of the diversity and ecology of modern MTB, coupled with detailed characterizations of the size/shape/arrangement of their biomineralized magnetite, are needed to build on the foundation provided here to develop biogeochemical paleoenvironmental proxies from the magnetofossil record.

Materials and methods

Sediment sampling, MTB collection, and sample preparation

Surface sediments were collected from nine locations from freshwater, brackish, and marine environments in China (Table S1). The collected sediments were transferred

15

into 500-ml plastic bottles with a 2:1 sediment to water ratio. The bottles were shipped to the laboratory and were stored at ~20°C in dim light to set up the laboratory microcosms. MTB in the microcosms were checked routinely with the hanging-drop technique (Schüler, 2002) using an Olympus BX51 microscope equipped with phase-contrast, fluorescence, and a DP70 digital camera system (Olympus Corp., Tokyo, Japan). Sufficient living MTB cells of interest were extracted magnetically from the sediments, washed three times with Milli-Q water, and were then divided into three parts for TEM, molecular, and FISH-SEM experiments, respectively, following the protocol of Li *et al.* (2017).

Molecular experiments

PCR amplification of 16S rRNA genes of MTB cells was performed using the universal bacterial primers 27F (5-′AGAGTTTGATCCTGGCTCAG-3′) and 1492R (5′-GGTTACCTTGTTACGACTT-3′) (Lane, 1991), following the protocol of Li *et al.* (2017). PCR products were purified using an EZNAR Gel Extraction Kit (Omega Bio-tek, Inc., USA). They are ligated with the pMD19-T vector (TaKaRa, Japan), then cloned in *Escherichia coli* (strain DH5α) competent cells (Tiangen, Beijing, China) according to the manufacturer's instructions. For each microcosm, 10-80 clones were picked randomly and were sequenced using the vector primers M13-47 (5′-CGCCAGGGTTTTCCCAGTCACGAC-3′) and RV-M (5′-GAGCGGATAACAATTTCACACAGG-3′) at the Huada Genome Center (Beijing, China). After discarding sequences of insufficient length (<1,300 bp), remaining sequences were aligned with close relatives using the ClustalW algorithm for manual correction. A phylogenetic tree was constructed using the maximum likelihood (ML) method (Tamura and Nei, 1993) in the MEGA software package (version 7.0) (Kumar *et al.*, 2016). Bootstrap values were calculated with 1,000 replicates.

16

Coupled FISH-SEM experiments and MTB identification

Nineteen species-specific oligonucleotide probes were designed to target specifically the corresponding 16S rRNA genes of magnetotactic cocci identified in this study (Table S2). Their probe specificity is given in Table S3. The universal bacteria probe EUB338 (5′-GCTGCCTCCCGTAGGAGT-3′) was used as a positive control probe of bacteria for FISH (Amann *et al.*, 1990; Li *et al.*, 2017). Probe EUB338 was synthesized and fluorescently labeled with fluorescein phosphoramidite FAM at the 5′ end, while all MTB species-specific probes were synthesized and labeled fluorescently with hydrophilic sulfoindocyanine dye Cy3 at the 5′ end. In some cases, *E. coli* or/and *Magnetospirillum magneticum* AMB-1 cells were added in appropriate amounts to the targeted magnetotactic cocci as inner control cells of non-magnetotactic *Gammaproteobacteria* or/and magnetotactic *Alphaproteobacteria*, respectively (Li *et al.*, 2017). Coupled FISH-SEM analysis was performed using the protocol described by Li *et al.* (2017). Fluorescence microscopy experiments were carried out using an Olympus BX51 microscope. After fluorescence microscope observations, the same sample was carbon-coated using a Leica ACE200 Low Vacuum Sputter Coater (Leica Microsystems, Wetzlar, Germany), and was observed using a Zeiss Ultra-55 field-emission gun SEM (Carl Zeiss, Germany) operating at 5 kV.

TEM Analysis

Conventional TEM observations were performed on a JEM2100 microscope (JEOL Ltd., Tokyo, Japan) operating at 200 kV at the Institute of Geology and Geophysics, Chinese Academy of Sciences (Beijing, China). Cell diameter, particle number, and crystal length (along the long axis) and width (perpendicular to the long axis) of the magnetite particles were measured from the TEM images of individual MTB cells. The axial ratio of particles is the width/length ratio. For each MTB strain,

17

at least 30 individual cells were selected randomly for statistical analysis of cell diameter and particle number, with at least 300 individual particles selected randomly for statistical analysis of crystal length and width. Chemical microanalysis was carried out with a JEM-2100F microscope (JEOL Ltd., Tokyo, Japan) operating at 200 kV at the Institut de minéralogie, de physique des matériaux et de cosmochimie (Paris, France). This microscope is equipped with a field emission gun, a JEOL detector with an ultrathin window, and a scanning TEM device. EDX elemental mapping was carried out in high-angle annular dark-field STEM mode.

Data processing and statistical analysis

Probability distribution analysis and 2D Kolmogorov-Smirnov tests were used to analyze crystal lengths, widths, and axial ratios to estimate differences in particle morphology among MTB species. To study quantitively the relationship between bacterial phylogeny and magnetosome biomineralization, nMDS analysis was performed using four physical features (particle number, chain configuration, crystal width, and axial ratio) using vegan, a package of community analysis functions for the statistical software R. NMDS is a rank-based method in which the original distance is substituted with ranks. The ranks of particle number, crystal width, and axial ratio for one certain MTB cell are obtained by normalized to the corresponding maximum values within all the test cells. For the chain configuration, the rank for two double chains, two chains, single chain, and non-chain were designed to 1.0, 0.5, 0.25, and 0, respectively. Permutational analysis of variance (PERMANOVA) (Anderson, 2001) was used to test for differences in magnetite biomineralization among MTB species. Envfit was further used to fit biomineralization vector features onto the nMDS ordination to determine average factor levels.

18

Data availability. The 16S rRNA gene sequences obtained here have been deposited in GenBank. Magnetotactic cocci strains MYC-3, MYC-4, MYC-5, MYC-7, DMHC-1, DMHC-2, DMHC-6, DMHC-8, WYHC-1, WYHC-2, WYHC-3, YQC-1, YQC-2, YQC-3, BHC-1, LLTC-1, SHHC-2, THC-1, and XJHC-1 are under accession numbers MN372077, MN372080, MN396678, MN396679, MN396579, MN396560, MN396584, MN396585, MN396452, MN396580, MN396581, MN396453, MN396538, MN396541, MN396586, MN396600, MN396451, MN396570, and MN396582, respectively.

Author contributions. JHL designed the research. PYL, YL, HZ, and FXW prepared samples and carried out microbiological experiments. JHL, PYL, and NM carried out TEM experiments. JHL, PYL, HZ, and FXW performed FISH-SEM experiments. JHL, PYL, XZ, YZ, and YL carried out data and statistical analysis. All authors participated in discussion of results. JHL and PYL prepared the manuscript.

19

References

Abreu, F., Carolina, A., Araujo, V., Leao, P., Silva, K. T., De Carvalho, F. M., Cunha, O. D. L., Almeida, L. G.*, et al.* (2016) Culture-independent characterization of novel psychrophilic magnetotactic cocci from Antarctic marine sediments. Environ Microbiol **18**: 4426-4441.

Amann, R. I., Krumholz, L. and Stahl, D. A. (1990) Fluorescent-oligonucleotide probing of whole cells for determinative, phylogenetic, and environmental studies in microbiology. J Bacteriol **172**: 762-770.

Anderson, M. J. (2001) A new method for non-parametric multivariate analysis of variance. Austral Ecol **26**: 32-46.

Bazylinski, D. A. and Frankel, R. B. (2004) Magnetosome formation in prokaryotes. Nat Rev Microbiol **2**: 217-230.

Bazylinski, D. A., Williams, T. J., Lefèvre, C. T., Berg, R. J., Zhang, C. L. L., Bowser, S. S., Dean, A. J. and Beveridge, T. J. (2013) *Magnetococcus marinus* gen. nov., sp nov., a marine, magnetotactic bacterium that represents a novel lineage (*Magnetococcaceae* fam. nov., *Magnetococcales* ord. nov.) at the base of the *Alphaproteobacteria*. Int J Syst Evol Microbiol **63**: 801-808.

Blakemore, R. P. (1975) Magnetotactic bacteria. Science **190**: 377-379.

Chang, L., Harrison, R. J., Zeng, F., Berndt, T. A., Roberts, A. P., Heslop, D. and Zhao, X. (2018) Coupled microbial bloom and oxygenation decline recorded by magnetofossils during the Palaeocene–Eocene Thermal Maximum. Nat Commun **9**: 4007.

Chang, S. B. R. and Kirschvink, J. L. (1989) Magnetofossils, the magnetization of sediments, and the evolution of magnetite biomineralization. Annu Rev Earth Planet Sci **17**: 169-195.

Chen, H., Li, J., Xing, X., Du, Z. and Chen, G. (2015) Unexpected diversity of magnetococci in intertidal sediments of Xiaoshi Island in the North Yellow Sea. J Nanomater **2015**: 902121.

Delong, E. F., Frankel, R. B. and Bazylinski, D. A. (1993) Multiple evolutionary origins

20

of magnetotaxis in bacteria. Science **259**: 803-806.

Devouard, B., Pósfai, M., Hua, X., Bazylinski, D. A., Frankel, R. B. and Buseck, P. R. (1998) Magnetite from magnetotactic bacteria: size distributions and twinning. Am Mineral **83**: 1387-1398.

Egli, R. (2004) Characterization of individual rock magnetic components by analysis of remanence curves. 3. Bacterial magnetite and natural processes in lakes. Phys Chem Earth **29**: 869-884.

Esser, C., Martin, W. and Dagan, T. (2007) The origin of mitochondria in light of a fluid prokaryotic chromosome model. Biol Lett **3**: 180-184.

Flies, C. B., Jonkers, H. M., De Beer, D., Bosselmann, K., Böttcher, M. E. and Schüler, D. (2005a) Diversity and vertical distribution of magnetotactic bacteria along chemical gradients in freshwater microcosms. FEMS Microbiol Ecol **52**: 185-195.

Flies, C. B., Peplies, J. and Schuler, D. (2005b) Combined approach for characterization of uncultivated magnetotactic bacteria from various aquatic environments. Appl Environ Microbiol **71**: 2723-2731.

He, K. and Pan, Y. X. (2020) Magnetofossil abundance and diversity as paleoenvironmental proxies: a case study from southwest Iberian margin sediments. Geophys Res Lett **47**: e2020GL087165.

Ji, B. Y., Zhang, S. D., Zhang, W. J., Rouy, Z., Alberto, F., Santini, C.-L., Mangenot, S., Gagnot, S.*, et al.* (2017) The chimeric nature of the genomes of marine magnetotactic coccoid-ovoid bacteria defines a novel group of *Proteobacteria*. Environ Microbiol **19**: 1103-1119.

Jovane, L., Florindo, F., Bazylinski, D. A. and Lins, U. (2012) Prismatic magnetite magnetosomes from cultivated Magnetovibrio blakemorei strain MV-1: a magnetic fingerprint in marine sediments? Environ Microbiol Rep **4**: 664-668.

Katzmann, E., Scheffel, A., Gruska, M., Plitzko, J. M. and Schüler, D. (2010) Loss of the actin‐like protein MamK has pleiotropic effects on magnetosome formation and chain assembly in *Magnetospirillum gryphiswaldense*. Mol Microbiol **77**: 208-224.

21

Kirschvink, J. L. and Chang, S. B. R. (1984) Ultrafine-grained magnetite in deep-sea sediments: possible bacterial magnetofossils. Geology **12**: 559-562.

Kobayashi, A., Kirschvink, J. L., Nash, C. Z., Kopp, R. E., Sauer, D. A., Bertani, L. E., Voorhout, W. F., and Taguchi, T. (2006), Experimental observation of magnetosome chain collapse in magnetotactic bacteria: sedimentological, paleomagnetic, and evolutionary implications. Earth Planet Sci Lett, **245**: 538-550.

Kolinko, S., Jogler, C., Katzmann, E., Wanner, G., Peplies, J. and Schüler, D. (2012) Single-cell analysis reveals a novel uncultivated magnetotactic bacterium within the candidate division OP3. Environ Microbiol **14**: 1709-1721.

Kolinko, S., Wanner, G., Katzmann, E., Kiemer, F., Fuchs, B. M. and Schüler, D. (2013) Clone libraries and single cell genome amplification reveal extended diversity of uncultivated magnetotactic bacteria from marine and freshwater environments. Environ Microbiol **15**: 1290-1301.

Komeili, A. (2012) Molecular mechanisms of compartmentalization and biomineralization in magnetotactic bacteria. FEMS Microbiol Rev **36**: 232-255.

Komeili, A., Vali, H., Beveridge, T. J. and Newman, D. K. (2004) Magnetosome vesicles are present before magnetite formation, and MamA is required for their activation. Proc Natl Acad Sci USA **101**: 3839-3844.

Kopp, R. E. and Kirschvink, J. L. (2008) The identification and biogeochemical interpretation of fossil magnetotactic bacteria. Earth-Sci Rev **86**: 42-61.

Koziaeva, V., Dziuba, M., Leão, P., Uzun, M., Krutkina, M. and Grouzdev, D. (2019) Genome-based metabolic reconstruction of a novel uncultivated freshwater magnetotactic coccus "*Ca.* Magnetaquicoccus inordinatus" UR-1, and proposal of a candidate Family "*Ca.* Magnetaquicoccaceae". Front Microbiol **10**: 2290.

Kozyaeva, V. V., Grouzdev, D. S., Dziuba, M. V., Kolganova, T. V. and Kuznetsov, B. B. (2017) Diversity of magnetotactic bacteria of the Moskva River. Microbiology **86**: 106-112.

Kumar, S., Stecher, G. and Tamura, K. (2016) MEGA7: molecular evolutionary genetics analysis version 7.0 for bigger datasets. Mol Biol Evol **33**: 1870-1874.

22

Lane, D. J. (1991) 16S/23S rRNA sequencing. In: Nucleic Acid Techniques in Bacterial Systematics. Wiley J. and Sons (ed), New York, pp. 115–175.

Larrasoaña, J. C., Liu, Q. S., Hu, P. X., Roberts, A. P., Mata, P., Civis, J., Sierro, F. J. and Perez-Asensio, J. N. (2014) Paleomagnetic and paleoenvironmental implications of magnetofossil occurrences in late Miocene marine sediments from the Guadalquivir Basin, SW Spain. Front Microbiol **5**: 71.

Leão, P., Le Nagard, L., Yuan, H., Cypriano, J., Da Silva-Neto, I., Bazylinski, D. A., Acosta-Avalos, D., De Barros, H. L.*, et al.* (2020) Magnetosome magnetite biomineralization in a flagellated protist: evidence for an early evolutionary origin for magnetoreception in eukaryotes. Environ Microbiol **22**: 1495-1506.

Lefèvre, C. T. and Bazylinski, D. A. (2013) Ecology, diversity, and evolution of magnetotactic bacteria. Microbiol Mol Biol Rev **77**: 497-526.

Lefèvre, C. T., Bernadac, A., Yu-Zhang, K., Pradel, N. and Wu, L. F. (2009) Isolation and characterization of a magnetotactic bacterial culture from the Mediterranean Sea. Environ Microbiol **11**: 1646-1657.

Lefèvre, C. T., Pósfai, M., Abreu, F., Lins, U., Frankel, R. B. and Bazylinski, D. A. (2011) Morphological features of elongated-anisotropic magnetosome crystals in magnetotactic bacteria of the *Nitrospirae phylum* and the *Deltaproteobacteria* class. Earth Planet Sci Lett **312**: 194-200.

Li, J. H., Benzerara, K., Bernard, S. and Beyssac, O. (2013a) The link between biomineralization and fossilization of bacteria: insights from field and experimental studies. Chem Geol **359**: 49-69.

Li, J. H., Ge, K. P., Pan, Y. X., Williams, W., Liu, Q. S. and Qin, H. F. (2013b) A strong angular dependence of magnetic properties of magnetosome chains: implications for rock magnetism and paleomagnetism. Geochem Geophys Geosyst **14**: 3887-3907.

Li, J. H., Menguy, N., Gatel, C., Boureau, V., Snoeck, E., Patriarche, G., Leroy, E. and Pan, Y. X. (2015) Crystal growth of bullet-shaped magnetite in magnetotactic bacteria of the *Nitrospirae* phylum. J R Soc Interface **12**: 20141288.

Li, J. H., Menguy, N., Roberts, A. P., Gu, L., Leroy, E., Bourgon, J., Yang, X. A., Zhao,

X., Liu, P. Y., Changela, H., and Pan, Y. X. (2020), Bullet-shaped magnetite biomineralization within a magnetotactic Deltaproteobacterium: implications for magnetofossil identification, J Geophys Res-Biogeo, **125**: e2020JG005680.

Li, J. H., Zhang, H., Liu, P. Y., Menguy, N., Roberts, A. P., Chen, H. T., Wang, Y. Z. and Pan, Y. X. (2019) Phylogenetic and structural identification of a novel magnetotactic *Deltaproteobacteria* strain, WYHR-1, from a freshwater lake. Appl Environ Microbiol **85**: e00731-19.

Li, J. H., Zhang, H., Menguy, N., Benzerara, K., Wang, F. X., Lin, X. T., Chen, Z. B. and Pan, Y. X. (2017) Single-cell resolution of uncultured magnetotactic bacteria via fluorescence-coupled electron microscopy. Appl Environ Microbiol **83**: e00409-17.

Lin, W., Bazylinski, D.A., Xiao, T., Wu, L.-F., and Pan, Y.X. (2014) Life with compass: diversity and biogeography of magnetotactic bacteria. Environ Microbiol **16**: 2646-2658.

Lin, W., Kirschvink, J. L., Paterson, G. A., Bazylinski, D. A. and Pan, Y. X. (2019) On the origin of microbial magnetoreception. Natl Sci Rev **7**: 472-479.

Lin, W., Li, J. H., Schueler, D., Jogler, C. and Pan, Y. X. (2009) Diversity analysis of magnetotactic bacteria in Lake Miyun, northern China, by restriction fragment length polymorphism. Syst Appl Microbiol **32**: 342-350.

Lin, W. and Pan, Y. X. (2009) Uncultivated magnetotactic cocci from Yuandadu park in Beijing, China. Appl Environ Microbiol **75**: 4046-4052.

Lin, W. and Pan, Y. X. (2010) Temporal variation of magnetotactic bacterial communities in two freshwater sediment microcosms. FEMS Microbiol Lett **302**: 85-92.

Lin, W., Paterson, G. A., Zhu, Q. Y., Wang, Y. Z., Kopylova, E., Li, Y., Knight, R., Bazylinski, D. A.*, et al.* (2017) Origin of microbial biomineralization and magnetotaxis during the Archean. Proc Natl Acad Sci USA **114**: 2171-2176.

Lin, W., Zhang, W. S., Zhao, X., Roberts, A. P., Paterson, G. A., Bazylinski, D. A. and Pan, Y. X. (2018) Genomic expansion of magnetotactic bacteria reveals an early common origin of magnetotaxis with lineage-specific evolution. ISME J **12**:

24

1508-1519.

Lins, U., McCartney, M. R., Farina, M., Frankel, R. B. and Buseck, P. R. (2006) Crystal habits and magnetic microstructures of magnetosomes in coccoid magnetotactic bacteria. An Acad Bras Ciênc **78**: 463-474.

Mann, S., Frankel, R. B. and Blakemore, R. P. (1984) Structure, morphology and crystal growth of bacterial magnetite. Nature **310**: 405-407.

Meldrum, F. C., Mann, S., Heywood, B. R., Frankel, R. B. and Bazylinski, D. A. (1993a) Electron microscopy study of magnetosomes in a cultured Coccoid magnetotactic bacterium. Proc R Soc Lond B **251**: 231-236.

Meldrum, F. C., Mann, S., Heywood, B. R., Frankel, R. B. and Bazylinski, D. A. (1993b) Electron microscopy study of magnetosomes in two cultured Vibrioid magnetotactic bacteria. Proc R Soc Lond B **251**: 237-242.

Monteil, C. L., Vallenet, D., Menguy, N., Benzerara, K., Barbe, V., Fouteau, S., Cruaud, C., Floriani, M.*, et al.* (2019) Ectosymbiotic bacteria at the origin of magnetoreception in a marine protist. Nat Microbiol **4**: 1088-1095.

Morillo, V., Abreu, F., Araujo, A. C., De Almeida, L. G. P., Enrich-Prast, A., Farina, M., De Vasconcelos, A. T. R., Bazylinski, D. A. and Lins, U. (2014) Isolation, cultivation and genomic analysis of magnetosome biomineralization genes of a new genus of south-seeking magnetotactic cocci within the *Alphaproteobacteria*. Front Microbiol **5**: 72.

Murat, D., Quinlan, A., Vali, H. and Komeili, A. (2010) Comprehensive genetic dissection of the magnetosome gene island reveals the step-wise assembly of a prokaryotic organelle. Proc Natl Acad Sci USA **107**: 5593-5598.

Muxworthy, A. R. and Williams, W. (2009) Critical superparamagnetic/single-domain grain sizes in interacting magnetite particles: implications for magnetosome crystals. J R Soc Interface **6**: 1207-1212.

Pan, H. M., Zhu, K. L., Song, T., Yu-Zhang, K., Lefèvre, C., Xing, S., Liu, M., Zhao, S. J.*, et al.* (2008) Characterization of a homogeneous taxonomic group of marine magnetotactic cocci within a low tide zone in the China Sea. Environ Microbiol **10**: 1158-1164.

25

Pósfai, M., Lefèvre, C. T., Trubitsyn, D., Bazylinski, D. A. and Frankel, R. B. (2013) Phylogenetic significance of composition and crystal morphology of magnetosome minerals. Front Microbiol **4**: 344.

Pósfai, M., Moskowitz, B. M., Arato, B., Schuler, D., Flies, C., Bazylinski, D. A. and Frankel, R. B. (2006) Properties of intracellular magnetite crystals produced by *Desulfovibrio magneticus* strain RS-1. Earth Planet Sci Lett **249**: 444-455.

Qian, X. X., Liu, J., Menguy, N., Li, J. H., Alberto, F., Teng, Z. J., Xiao, T., Zhang, W. Y. and Wu, L. F. (2019) Identification of novel species of marine magnetotactic bacteria affiliated with *Nitrospirae* phylum. Environ Microbiol Rep **11**: 330-337.

Qian, X. X., Santini, C. L., Kosta, A., Menguy, N., Le Guenno, H., Zhang, W. Y., Li, J. H., Chen, Y. R.*, et al.* (2020) Juxtaposed membranes underpin cellular adhesion and display unilateral cell division of multicellular magnetotactic prokaryotes. Environ Microbiol **22**: 1481-1494.

Roberts, A. P., Florindo, F., Villa, G., Chang, L., Jovane, L., Bohaty, S. M., Larrasoaña, J. C., Heslop, D. and Fitz Gerald, J. D. (2011) Magnetotactic bacterial abundance in pelagic marine environments is limited by organic carbon flux and availability of dissolved iron. Earth Planet Sci Lett **310**: 441-452.

Rodelli, D., Jovane, L., Roberts, A. P., Cypriano, J., Abreu, F. and Lins, U. (2018) Fingerprints of partial oxidation of biogenic magnetite from cultivated and natural marine magnetotactic bacteria using synchrotron radiation. Environ Microbiol Rep **10**: 337-343.

Sakuramoto, Y., Yamazaki, T., Kimoto, K., Miyairi, Y., Kuroda, J., Yokoyama, Y. and Matsuzaki, H. (2017) A geomagnetic paleointensity record of 0.6 to 3.2 Ma from sediments in the western equatorial Pacific and remanent magnetization lock-in depth. J Geophys Res: Solid Earth **122**: 7525-7543.

Savian, J. F., Jovane, L., Frontalini, F., Trindade, R. I. F., Coccioni, R., Bohaty, S. M., Wilson, P. A., Florindo, F.*, et al.* (2014) Enhanced primary productivity and magnetotactic bacterial production in response to middle Eocene warming in the Neo-Tethys Ocean. Paleogeogr Paleoclimatol Paleoecol **414**: 32-45.

Savian, J. F., Jovane, L., Giorgioni, M., Iacoviello, F., Rodelli, D., Roberts, A. P., Chang, L., Florindo, F. and Sprovieri, M. (2016) Environmental magnetic implications of magnetofossil occurrence during the Middle Eocene Climatic Optimum (MECO) in pelagic sediments from the equatorial Indian Ocean. Paleogeogr Paleoclimatol Paleoecol **441**: 212-222.

Scheffel, A., Gardes, A., Grunberg, K., Wanner, G. and Schüler, D. (2008) The major magnetosome proteins MamGFDC are not essential for magnetite biomineralization in *Magnetospirillum gryphiswaldense* but regulate the size of magnetosome crystals. J Bacteriol **190**: 377-386.

Scheffel, A., Gruska, M., Faivre, D., Linaroudis, A., Plitzko, J. M. and Schüler, D. (2006) An acidic protein aligns magnetosomes along a filamentous structure in magnetotactic bacteria. Nature **440**: 110-114.

Schübbe, S., Williams, T. J., Xie, G., Kiss, H. E., Brettin, T. S., Martinez, D., Ross, C. A., Schüler, D.*, et al.* (2009) Complete genome sequence of the chemolithoautotrophic marine *Magnetotactic Coccus* strain MC-1. Appl Environ Microbiol **75**: 4835-4852.

Schüler, D. (2002) The biomineralization of magnetosomes in *Magnetospirillum gryphiswaldense*. Int Microbiol **5**: 209-214.

Singer, E., Emerson, D., Webb, E. A., Barco, R. A., Kuenen, J. G., Nelson, W. C., Chan, C. S., Comolli, L. R.*, et al.* (2011) *Mariprofundus ferrooxydans* PV-1 the first genome of a marine Fe (II) oxidizing *Zetaproteobacterium*. PLoS One **6**: e25386.

Siponen, M. I., Legrand, P., Widdrat, M., Jones, S. R., Zhang, W.-J., Chang, M. C. Y., Faivre, D., Arnoux, P. and Pignol, D. (2013) Structural insight into magnetochrome-mediated magnetite biomineralization. Nature **502**: 681-684.

Spring, S., Amann, R., Ludwig, W., Schleifer, K. H. and Petersen, N. (1992) Phylogenetic diversity and identification of nonculturable magnetotactic bacteria. Syst Appl Microbiol **15**: 116-122.

Spring, S., Amann, R., Ludwig, W., Schleifer, K. H., Schüler, D., Poralla, K. and Petersen, N. (1995) Phylogenetic analysis of uncultured magnetotactic bacteria

from the alpha-subclass of *Proteobacteria*. Syst Appl Microbiol **17**: 501-508.

Spring, S., Lins, U., Amann, R., Schleifer, K., Ferreira, L., Esquivel, D. and Farina, M. (1998) Phylogenetic affiliation and ultrastructure of uncultured magnetic bacteria with unusually large magnetosomes. Arch Microbiol **169**: 136-147.

Staniland, S. S. and Rawlings, A. E. (2016) Crystallizing the function of the magnetosome membrane mineralization protein Mms6. Biochem Soc Trans **44**: 883-890.

Tamura, K. and Nei, M. (1993) Estimation of the number of nucleotide substitutions in the control region of mitochondrial DNA in humans and chimpanzees. Mol Biol Evol **10**: 512-526.

Toro-Nahuelpan, M., Giacomelli, G., Raschdorf, O., Borg, S., Plitzko, J. M., Bramkamp, M., Schüler, D. and Müller, F.-D. (2019) MamY is a membrane-bound protein that aligns magnetosomes and the motility axis of helical magnetotactic bacteria. Nat Microbiol **4**: 1978-1989.

Uebe, R. and Schüler, D. (2016) Magnetosome biogenesis in magnetotactic bacteria. Nat Rev Microbiol **14**: 621-637.

Usui, Y., Yamazaki, T. and Saitoh, M. (2017) Changing abundance of magnetofossil morphologies in pelagic red clay around Minamitorishima, western North Pacific. Geochem Geophys Geosyst **18**: 4558-4572.

Wang, Y. Z., Lin, W., Li, J. H. and Pan, Y. X. (2013) High diversity of magnetotactic *Deltaproteobacteria* in a freshwater niche. Appl Environ Microbiol **79**: 2813-2817.

Yamazaki, T. and Kawahata, H. (1998) Organic carbon flux controls the morphology of magnetofossils in marine sediments. Geology **26**: 1064-1066.

Yamazaki, T., Suzuki, Y., Kouduka, M. and Kawamura, N. (2019) Dependence of bacterial magnetosome morphology on chemical conditions in deep-sea sediments. Earth Planet Sci Lett **513**: 135-143.

Zhang, H., Menguy, N., Wang, F. X., Benzerara, K., Leroy, E., Liu, P. Y., Liu, W. Q., Wang, C. L*., et al.* (2017) Magnetotactic coccus strain SHHC-1 affiliated to *Alphaproteobacteria* forms octahedral magnetite magnetosomes. Front

28

Microbiol **8**: 969.

29

Figure and Table Captions

Figure 1. Phylogenetic and structural identification of representative magnetotactic cocci strains A-D. BHC-1, E-H. LLTC-1, I-L. DMHC-2, and M-P. MYC-3 using the coupled FISH-SEM approach. First column: fluorescence microscope maps (false colour) of bacteria hybridized by the 5′-FAM-labeled universal bacterial probe EUB338. Second column: fluorescence microscope maps (false colour) of bacteria hybridized by the 5′-Cy3-labeled species-specific probes. Third column: SEM images of the same area as in the first column. Forth column: high-magnification SEM image of targeted magnetotactic cocci marked by dashed boxes in the third column.

Figure 2. Phylogenetic position and morphology of magnetotactic cocci identified in this study. Blue background represents strains affiliated with the *Magnetococcales* order. A. Phylogenetic tree based on 16S rRNA gene sequences with the positions of magnetotactic cocci identified in this study in the *Magnetoccales* order. Bootstrap values at nodes are percentages of 1,000 replicates. The 16S rRNA gene sequence of the magnetotactic bacteria *Candidatus* Omnitrophus magneticus SKK-01 was used to root the tree. GenBank accession numbers are given in parentheses. B-U. TEM images of strains B. YQC-1, C. BHC-1, D. YQC-2, E. MYC-4, F. XJHC-1, G. LLTC-1, H. WYHC-2, I. SHHC-1, J. DMHC-1, K. WYHC-1, L. THC-1, M. MYC-5, N. DMHC-8, O. YQC-3, P. DMHC-2, Q. MYC-3, R. MYC-7, S. DMHC-6, T. WYCH-3, and U. SHHC-2. Strain SHHC-1 (indicated by the * symbol) was discovered in our previous study (Zhang *et al.*, 2017) from the same location as strain SHHC-2 and was used in this study for phylogenetic analysis and morphological comparison.

Figure 3. Cumulative probability distributions for magnetosomal magnetite length (first column), width (second column), and width to length ratio (axial ratio) (third column). The mean (colored solid line) and 95% confidence level (colored band) of

30

each strain is estimated from 10,000 Monte Carlo simulations, which are further used to investigate the similarity of grain-size distributions of any two strains with a Kolmogorov-Smirnov test (Supplementary Material S2). A. Magnetotactic cocci with a single magnetite chain (for strains WHC-3, YQC-2, YQC-1, WYHC-1, and DMHC-1). B. Magnetotactic cocci with double chains (for strains YQC-3, XJHC-1, MYC-5, MYC-4, and LLTC-1). C. Magnetotactic cocci with two double chains (for strains DMHC-2, SHHC-1, and DMHC-8). D. Magnetotactic cocci with non-chain structure (for strains SHHC-2, DMHC-6, THC-1, MYC-7, WYHC-2, and MYC-3).

Figure 4. Phylogenetic distribution of MTB (black and red solid circles) and non-MTB (white empty circles) in the *Candidatus* Etaproteobacteria, *Alphaproteobacteria*, *Betaproteobacteria*, *Gammaproteobacteria*, *Deltaproteobacteria*, and *Epsilonproteobacteria* classes of the *Proteobacteria* phylum, the *Nitrospirae* phylum, and the *Candidatus* Omnitrophica phylum. Magnetotactic cocci strains identified in this study are marked by red solid circles.

Figure 5. Non-metric multidimensional scaling (nMDS) ordination plot of magnetosomal magnetite features (chain configuration, particle number, crystal width, and axial ratio) for magnetotactic cocci, using Euclidean distance and stress = 0.07. Data for individual cells of the same MTB species cluster together, while data for MTB species with the same chain configuration cluster in a small area.

Table 1. Morphological features of magnetotactic bacteria and their magnetosomal magnetite particles identified in this study.

Supplementary Figure S1. Chemical microanalysis of magnetosomes using STEM-EDX mapping in the high-angle annular dark-field (HAADF) mode. A. HAADF-

31

STEM image of two MYC-4 cells and one unknown MTB cell, and corresponding chemical maps for B. C (C Kα), C. S (S Kα), and D. Fe (Fe Kα). E. RGB map with Fe (red), C (blue), and S (green). F. HAADF-STEM image of a DMHC-8 cell, and corresponding chemical maps of G. P (P Kα), H. S (S Kα), and I. Fe (Fe Kα). J. RGB map with Fe (red), P (blue), and S (green). K. EDX spectra for the carbon film covering the TEM grid (black), cell wall (indigo), magnetosomal magnetite particles (red), sulfur particle (green), and polyphosphate inclusion (blue).

Supplementary Figure S2. Morphological features of magnetosomal magnetite produced by six different magnetotactic cocci with a single chain configuration. TEM images of magnetite in strains A. BHC-1, B. YQC-1, C. YQC-2, D. WYHC-1, E. WYHC-3, and F. DMHC-1. Box-whisker plots of G. crystal length, H. width, and I. axial ratio of magnetite crystals, which reveal morphological differences among the strains.

Supplementary Figure S3. Morphological features of magnetosomal magnetite produced by five different magnetotactic cocci with a double chain configuration. TEM images of magnetite in strains A. MYC-4, B. MYC-5, C. YQC-3, D. LLTC-1, and E. XJHC-1. Box-whisker plots of F. crystal length, G. width, and H. axial ratio of magnetite crystals, which reveal morphological differences among the strains.

Supplementary Figure S4. Morphological features of magnetosomal magnetite produced by three different magnetotactic cocci with two double chain configurations. TEM images of magnetite in strains A. DMHC-1, B. DMHC-8, and C. SHHC-1. Box-whisker plots of D. crystal length, E. width, and F. axial ratio of magnetite crystals, which reveal morphological differences among the strains. Strain SHHC-1 (indicated by the * symbol) was discovered in our previous study (Zhang *et al.*, 2017).

Supplementary Figure S5. Morphological features of magnetosomal magnetite

produced by six different magnetotactic cocci with non-chain configuration. TEM images of magnetite in strains A. MYC-3, B. MYC-7, C. WYHC-2, D. THC-1, E. DMHC-6, and F. SHHC-2. Box-whisker plots of G. crystal length, H. width, and I. axial ratio of magnetite crystals, which reveal morphological differences among the strains.

Supplementary Figure S6. Grain size distribution of magnetite particles from magnetotactic cocci identified in this study. Boundaries between the single domain (SD), multi-domain (MD), and superparamagnetic (SP) regions are from Muxworthy and Williams (Muxworthy and Williams, 2009).

Supplementary Figure S7. Variability of morphological feature vectors for magnetite particles in magnetotactic cocci based on nMDS ordination results (9,999 permutations) by Envfit. The function of Envfit is fitting feature vectors or factors onto an ordination. The projections of points onto vectors have maximum correlation with corresponding environmental variables, and the factors show the averages of factor levels. Clearly, the MDS1 axis principally represents crystal width, width/length ratio, and chain configuration, while the MDS2 axis principally represents the number of magnetite particles in the cell.

Supplementary Table S1. Sampling locations and environmental factors at the time of sampling.

Supplementary Table S2. FISH probes used in this study.

Supplementary Table S3. Mismatched information of FISH probes used in this study.

Supplementary Table S4. 16S rRNA sequences retrieved from selected laboratory microcosms.

33

Supplementary Materials

Supplementary Material S1. Phylogenetic and structural identification of magnetotactic cocci using the coupled FISH-SEM approaches.

Supplementary Material S2. Two-samples Kolmogorov-Smirnov test of the length, width, and axial ratio of biogenic magnetite particles within magnetotactic cocci.

Supplementary Material S3. PERMANOVA results of magnetosomal magnetite biomineralization features (particle number, chain configuration, crystal width and width/length ratio) of 20 magnetotactic cocci strains by pairwise comparison. Strains marked in yellow represent MTB species with the same chain configuration. In contrast, the others represent MTB species with different chain configurations. Group 1 and group 2 are the two comparison strains. Proportion of variance is the percentage of variance of the four biomineralization features.

34

Table 1. Morphological features of magnetotactic bacteria and their magnetosomal magnetite particles identified in this study.

MTB strain	Sampling site	Cell diameter (μm)	Magnetite particle number per cell	Chain configuration	2D projection/Shape	Length (nm)	Width (nm)	Axial Ratio	Similar 16S rRNA	Identity (%)	Reference
MYC-3	Miyun Lake	1.4±0.2	19±4	Dispersed aggregates	Elongated prismatic	74.6±10.5	50.3±7.2	0.68	HCH5049	99	(Wang *et al.*, 2013)
MYC-4		1.4±0.2	11±2	Double chains	Elongated prismatic	103.2±21.9	66.7±14.5	0.65	--	--	This study
MYC-5		2.2±0.3	33±6	Double chains	Octahedral	99.1±26.8	94.1±25.7	0.95	--	--	This study
MYC-7		1.2±0.2	10±2	Dispersed aggregates	Elongated prismatic	72.4±11.1	36.5±5.7	0.51	OTU8	98	(Lin and Pan 2010)
DMHC-1	Daming Lake	1.3±0.2	10±2	Single chain	Elongated prismatic	96.4±26.0	74.5±22.5	0.77	OTU2	97	(Lin and Pan 2010)
DMHC-2		1.3±0.2	29±6	Two double chains	Elongated Cubo-octahedral	74.0±19.4	57.1±16.2	0.77	--	--	This study
DMHC-6		2.1±0.2	70±13	Dispersed aggregates and partial chains	Elongated prismatic	69.3±8.7	45.7±5.6	0.66	--	--	This study
DMHC-8		1.8±0.2	42±8	Two double chains	Elongated prismatic	89.1±22.6	71.5±20.6	0.80	OTU17	99	(Lin and Pan 2010)
WYHC-1	Weiyang Lake	1.8±0.2	13±3	Single chain	Elongated prismatic	87.1±21.6	63.4±16.6	0.71	--	--	This study
WYHC-2		2.5±0.2	103±16	Dispersed aggregates	Elongated prismatic	73.9±10.1	41.2±6.5	0.56	--	--	This study
WYHC-3		1.2±0.1	12±3	Single chain	Cubo-octahedral	60.0±13.4	56.9±13.4	0.95	--	--	This study
YQC-1	Yuqiao Lake	1.9±0.3	10±3	Single chain	Elongated prismatic	72.6±21.4	36.1±10.1	0.50	clone 7	98	(Lin *et al.*, 2009)
YQC-2		1.6±0.2	10±2	Single chain	Elongated prismatic	74.5±15.9	52.9±11.8	0.71	--	--	This study
YQC-3		1.3±0.1	10±2	Double chains	Elongated prismatic	86.6±26.1	60.6±18.9	0.70	OTU29	99	(Lin and Pan 2010)
BHC-1	Beihai Lake	1.3±0.2	8±2	Single chain	Elongated prismatic	91.6±23.2	67.9±17.4	0.74	--	--	This study
THC-1	Tanghe River	2.5±0.2	35±15	Dispersed aggregates	Hexagonal prim	70.6±8.6	42.3±5.2	0.60	CF22	99	(Flies *et al.*, 2005)
SHHC-1*	Shihe Estuary	2.1±0.4	38±17	Two double chains	Elongated octahedron	83.3±19.2	69.9±17.3	0.84	WHI-8	97	(Chen *et al.*, 2015)
SHHC-2		1.7±0.2	30±7	Clusters and partial chains	Elongated prismatic	61.1±18.8	39.4±12.6	0.64	--	--	This study
LLTC-1	Laolongtou Bay	1.7±0.3	24±7	Double chains	Elongated prismatic	113.6±38.9	85.6±30.6	0.75	rj12	98	(Spring *et al.*, 1998)
XJHC-1	Xiajiahe Bay	1.0±0.1	13±3	Double chains	Elongated prismatic	98.8±20.9	73.9±17.1	0.75	--	--	This study

Notes: The Miyun (MY) and Beihai (BH) lakes are located in Beijing city, Yuqiao (YQ) Lake is in Tianjing city, Tanghe (TH) River, Shihe (SHH) Estuary, and Laolongtou (LLT) Bay are located in Qinghuangdao city (Hebei Province), Daminghu (DMH) Lake is in Jinan city (Shandong Province), Weiyanghu Lake (WYH) is in Xi'an city (Shannxi Province), and Xiajiahe (XJH) Bay is in Dalian city (Liaoning Province). The MY, BH, DMH, and YQ lakes, and TH river localities are in freshwater environments. The SHH Estuary represents a brackish environment, while the LLT and XJH bays are marine environments. More detailed information about sampling sites is given in Table S1. Values for cell diameter, magnetite particle number per cell, and magnetite particle size are given as the mean (before the ± symbol) and corresponding standard deviation (after the ± symbol). Among the 19 MTB strains identified in this study, ten are novel, while eight have been reported in previous studies based on their 16S rRNA gene sequences (sequence identify >97%). However, all 19 strains have been identified phylogenetically and structurally for the first time in the present study. The SHHC-1 strain (indicated by the * symbol) was identified by our group in a previous study and is also listed here for comparison (Zhang *et al.*, 2017).